



PCCP

**Infrared Multiple-Photon Dissociation Spectroscopy of
Cationized Glycine: Effects of Alkali Metal Cation Size on
Gas-Phase Conformation**

Journal:	<i>Physical Chemistry Chemical Physics</i>
Manuscript ID	CP-ART-07-2022-003469.R1
Article Type:	Paper
Date Submitted by the Author:	09-Sep-2022
Complete List of Authors:	Armentrout, Peter; University of Utah, Chemistry Stevenson, Brandon; University of Utah, Chemistry Ghiassee, Maryam ; University of Utah, Chemistry Boles, Georgia; University of Utah, Chemistry Berden, Giel; Radboud University, Institute for Molecules and Materials Oomens, Jos; Radboud University Nijmegen, Institute for Molecules and Materials

SCHOLARONE™
Manuscripts

Infrared Multiple-Photon Dissociation Spectroscopy of Cationized Glycine: Effects of Alkali Metal Cation Size on Gas-Phase Conformation

P. B. Armentrout,[†] Brandon C. Stevenson,[†] Maryam Ghiassaei,[†] Georgia C. Boles,[†] Giel Berden,[‡] and Jos Oomens^{‡§}

[†] Department of Chemistry, University of Utah, 315 South 1400 East, Room 2020, Salt Lake City, Utah 84112, United States

[‡] Radboud University, FELIX Laboratory, Institute for Molecules and Materials, Toernooiveld 7, NL-6525 ED Nijmegen, The Netherlands

[§] van't Hoff Institute for Molecular Sciences, University of Amsterdam, Science Park 904, NL-1098 XH Amsterdam, The Netherlands

Abstract: The gas-phase structures of cationized glycine (Gly), including complexes with Li⁺, Na⁺, K⁺, Rb⁺, and Cs⁺, are examined using infrared multiple-photon dissociation (IRMPD) spectroscopy utilizing light generated by a free electron laser, in conjunction with ab initio calculations. To identify the structures present in the experimental studies, measured IRMPD spectra are compared to spectra calculated at B3LYP/6-311+G(d,p) for the Li⁺, Na⁺, and K⁺ complexes and at B3LYP/def2TZVP for the Rb⁺ and Cs⁺ complexes. Single-point energy calculations were carried out at the B3LYP, B3P86, and MP2(full) levels using the 6-311+G(2d,2p) basis set for Li⁺, Na⁺, K⁺ and the def2TZVPP basis set for Rb⁺ and Cs⁺. The Li⁺ and Na⁺ complexes are identified as metal cation coordination to the amino nitrogen and carbonyl oxygen, [N,CO]-tt, although Na⁺(Gly) may have contributions from additional structures. The heavier metal cations coordinate to either the carbonyl oxygen, [CO]-cc, or the carbonyl oxygen and hydroxy oxygen, [CO,OH]-cc, with the former apparently preferred for Rb⁺ and Cs⁺ and the latter for K⁺. These two structures reside in a double-well potential and different levels of theory predict very different relative stabilities. Some experimental evidence is provided that MP2(full) theory provides the most accurate relative energies.

Introduction

The first infrared multiple-photon dissociation (IRMPD) spectroscopy study of metalated amino acids was conducted by Kapota et al., who examined the sodium cation complexes of glycine (Gly) and proline (Pro).¹ These two amino acids were chosen as the expectation was that the former complex would have charge-solvated coordination of the metal cation and the latter might show a zwitterionic complex. Indeed, the IRMPD spectra showed distinctive bands consistent with these expectations. Since then, IRMPD spectra of many of the naturally occurring amino acids (AAs) complexed with alkali cations have been obtained,²⁻²⁰ including a recent study of the sodiated aliphatic amino acids: Gly, alanine (Ala), homo-alanine (hAla), valine (Val), leucine (Leu), and isoleucine (Ile).²¹ In the latter work, the IRMPD spectrum of Na⁺(Gly) was retaken and found to be consistent with that of Kapota et al., but extended to lower wavenumbers (500 – 1850 cm⁻¹). In the present study, we examine effects of metal cation size on gas-phase conformations by measuring the IRMPD action spectra of Gly cationized by all five alkali cations: Li⁺, Na⁺, K⁺, Rb⁺, and Cs⁺. The conformations are identified by comparing the experimental spectra to IR spectra of the low-lying structures of the cationized Gly complexes predicted by quantum-chemical calculations at the B3LYP/6-311+G(d,p) level of theory for the lighter metals. For the heavy metal cations, Rb⁺ and Cs⁺, the B3LYP/def2TZVP approach is generally utilized throughout. As will be seen below, there is some ambiguity with regard to stable structures identified using the B3LYP density functional; therefore, MP2 and B3LYP with dispersion corrections (GD3BJ) are also explored for particular structures.

Previously, we have studied the interactions of Gly with all five alkali-metal cations using guided ion beam tandem mass spectrometry (GIBMS).²¹⁻²⁷ In each case, the metal cation binding energy to Gly was determined and possible structures of the M⁺(Gly) complexes were evaluated theoretically. In a recent reexamination of the potassiated complexes of the aliphatic AAs (including Gly),²⁷ we noted that there was a double-well potential between complexes in which K⁺ binds only to the carbonyl oxygen (designated [CO]-cc below) and to both oxygens ([CO,OH]-cc), where the latter also couples via a double-well potential to the zwitterionic form in which the

hydroxy proton has migrated to the amino group and K^+ binds to both carboxylate oxygens (designated $[CO_2^-]$ -cc below). Although all three conformers were theoretically characterized in that previous work, we carefully examine their relationship here again and extend the analysis to all five alkali cations.

Experimental and Computational section

Mass spectrometry and photodissociation

These experiments utilized a 4.7 T Fourier transform ion cyclotron resonance (FTICR) mass spectrometer, as described in detail elsewhere,²⁸⁻³⁰ Tunable radiation for the photodissociation experiments was generated at the free-electron lasers for infrared experiments (FELIX) laboratory at Radboud University in the Netherlands using the FELIX-2 beamline.³¹ For the present experiments, spectra were recorded over the wavenumber range of 600 – 1800 cm^{-1} . Pulse energies were in the range of 20 – 140 mJ per macropulse of 7 μs duration. The FWHM bandwidth of the laser was typically 0.5% of the central wavelength. Cationized amino acids were formed by electrospray ionization from a solution of 1.0 mM Gly and 1.0 mM alkali-metal chloride in 60:40% MeOH : H₂O. The IRMPD spectra for the metalated cation complexes were generated by calculating the photofragmentations yield, $Y = \sum I_F / (\sum I_P + \sum I_F)$, where I_P and I_F are the integrated intensities of precursor and fragment ion mass peaks (the sum includes all isotopes), respectively, as a function of the frequency of IR radiation. The signal plotted is then taken as $S = -\ln(1 - Y) = -\ln(\sum I_F / (\sum I_P + \sum I_F))$, which was then linearly corrected for frequency dependent variation in the laser pulse energy. The application of a linear laser power correction is well described in the literature³²⁻³³ and is appropriate because the power dependence is basically linear until saturation begins because of the incoherent rather than coherent nature of the multiple-photon excitation process. For complexes of Na^+ , Rb^+ , and Cs^+ , IRMPD yielded M^+ product ions. In the cases of Li^+ and K^+ complexes, no fragment ion was observed; hence, a depletion spectrum, defined as $S = -\ln(\sum I_P / \sum I_P^\circ)$, where I_P° is the integrated intensity of the precursor ion mass peak

without irradiation) was obtained instead. Here too, the signal was corrected for frequency-dependent variations in the laser pulse energy.

Computational Details

To determine the low-lying conformers of the cationized Gly complexes, the Gaussian16 suite of programs was used.³⁴ For Li^+ , Na^+ , and K^+ complexes, initial optimization of the metalated complexes were done at the B3LYP/6-31G(d) level of theory.³⁵⁻³⁶ Unique structures were then further optimized at the B3LYP/6-311+G(d,p) level of theory.³⁷⁻³⁸ This level of theory has been shown to provide reasonably accurate structural descriptions of comparable cationized-ligand systems.^{11-12, 14, 16, 19, 22-23} For Rb^+ and Cs^+ complexes, all atoms were described using the def2TZVP size-consistent basis set, which is a triple- ζ + polarization functions basis set with a small core (28 and 46 electrons, respectively) effective core potential (ECP) on Rb^+ and Cs^+ . The def2TZVP basis set and corresponding ECP were obtained from the EMSL basis set exchange.³⁹ Geometry optimizations of metalated structures were also conducted including corrections for empirical dispersion at the B3LYP-GD3BJ level using either the 6-311+G(d,p) or def2TZVP basis sets.⁴⁰⁻⁴¹ In select cases, geometries were also optimized at the MP2(full) level (where full refers to the correlation of all electrons), abbreviated as MP2 below, using the same basis sets.

Vibrational frequencies were scaled by 0.975 for comparison to the IRMPD spectra, where this scaling factor has been shown to account for known inaccuracies in the calculated frequencies, giving good agreement with well-resolved peaks in other IRMPD spectra. The calculated frequencies were broadened using a 50 cm^{-1} full width at half maximum Gaussian line shape when used for comparison to the experimentally determined spectra. The broadening accounts for the finite laser bandwidth, unresolved rotational envelope, anharmonic broadening of the vibrational bands, and broadening resulting from the multiple-photon absorption process. In select cases, we also conducted calculations of the anharmonic vibrational frequencies using the keyword “freq=anharmonic”. The anharmonic frequencies were left unscaled and broadened similarly to the harmonic calculations when compared to the experimental data.

Single-point energy calculations were carried out for the most stable structures at the B3LYP, B3P86, MP2, and in select cases, CCSD(T,full), levels of theory. For Li^+ , Na^+ , and K^+ complexes, the 6-311+G(2d,2p) basis set³⁷ was used, whereas for Rb^+ and Cs^+ complexes, the de2TZVPP basis was used. Zero-point vibrational energy (ZPE) and thermal corrections were determined using vibrational frequencies calculated at the B3LYP/6-311+G(d,p) or B3LYP/def2TZVP level and scaled by a factor of 0.989 to account for known inaccuracies.⁴²⁻⁴³ ZPE corrections were applied to single point energies in order to provide 0 K relative enthalpies. Thermal corrections to obtain 298 K Gibbs energies were calculated from 0 K relative enthalpies by using the rigid rotor/harmonic oscillator approximation with the calculated rotational constants and vibrational frequencies.

Results and Discussion

IRMPD action spectroscopy

Photodissociation spectra of $\text{M}^+(\text{Gly})$ species, where $\text{M} = \text{Li}^+$, Na^+ , K^+ , Rb^+ , and Cs^+ , were examined. For the Na^+ , Rb^+ , and Cs^+ complexes, photodissociation of the precursor ion results in the loss of the intact glycine ligand to form the atomic metal cation. This dissociation pathway is consistent with the only dissociation process observed in threshold collision-induced dissociation (TCID) spectra of $\text{Na}^+(\text{Gly})$, $\text{K}^+(\text{Gly})$, $\text{Rb}^+(\text{Gly})$, $\text{Cs}^+(\text{Gly})$.^{21-25, 27} As a result, the IRMPD action spectra for Na^+ , Rb^+ , and Cs^+ complexes of Gly were taken from the relative intensity of the M^+ product cation as a function of laser wavelength. For the $\text{Li}^+(\text{Gly})$ and $\text{K}^+(\text{Gly})$ species, loss of the metal cation was not observed. The Li^+ dissociation channel is beyond the accessible mass range of the FTICR MS, whereas the K^+ product was not observed because [an unresolved experimental artefact interferes at the ICR frequency corresponding to mass 39](#). As a result, the IRMPD action spectra on the FTICR for $\text{Li}^+(\text{Gly})$ and $\text{K}^+(\text{Gly})$ were taken from the depletion of the parent ion intensity as a function of laser wavelength.

Spectra for $\text{K}^+(\text{Gly})$, $\text{Rb}^+(\text{Gly})$, and $\text{Cs}^+(\text{Gly})$ were also acquired on a modified quadrupole ion trap (QIT) mass spectrometer (Bruker, Amazon Speed ETD),⁴⁴ with M^+ being observed as the

product ion in all cases (notably, in contrast to the FTICR results for the K^+ complex). These spectra are compared to those obtained using the FTICR in Figure S1 of the Supporting Information. In all three cases, the QIT spectra reproduce the major bands seen in the FTICR spectra; however, the latter also exhibit several minor bands and hence are used exclusively in the comparisons discussed below.

The IRMPD spectra of all five $M^+(\text{Gly})$ complexes are compared in Figure 1. It is evident that the spectra of $\text{Li}^+(\text{Gly})$ and $\text{Na}^+(\text{Gly})$ are similar, as are the spectra for $\text{K}^+(\text{Gly})$, $\text{Rb}^+(\text{Gly})$, and $\text{Cs}^+(\text{Gly})$. The most intense feature in all five spectra is a band near 1750 cm^{-1} , which red-shifts for the two lighter metal cations. $\text{Li}^+(\text{Gly})$, $\text{Na}^+(\text{Gly})$, $\text{Rb}^+(\text{Gly})$, and $\text{Cs}^+(\text{Gly})$ exhibit a band near 1600 cm^{-1} . The heavier metal complexes exhibit a band near 1380 cm^{-1} , whereas $\text{Li}^+(\text{Gly})$ shows two bands on either side of this (1280 and 1440 cm^{-1}) and $\text{Na}^+(\text{Gly})$ has intensity throughout this region. All five spectra exhibit weaker bands at ~ 1160 and $\sim 1060\text{ cm}^{-1}$. $\text{Li}^+(\text{Gly})$ and $\text{Na}^+(\text{Gly})$ have bands at 670 and 980 cm^{-1} that are absent for the three heavier complexes, which have bands at ~ 820 and $\sim 890\text{ cm}^{-1}$ that are not strong or absent for the lighter two complexes.

Theoretical Results

Detailed discussion of low-lying structures for Li^+ , Na^+ , K^+ , Rb^+ , and Cs^+ complexed with glycine can be found elsewhere.²¹⁻²⁷ Low-lying structures for $M^+(\text{Gly})$ complexes illustrated by the example of $M = \text{Rb}$ are shown in Figure 2. The nomenclature used to describe these cationized glycine conformations matches that used in these previous studies. Structures are identified by their metal binding sites in brackets (N = amino nitrogen, CO = carbonyl oxygen, OH = carboxylic acid hydroxy oxygen, CO_2^- = both oxygens of carboxylate) and followed by a description of the glycine amino acid backbone dihedral angles. Starting at the carboxylic acid hydrogen and ending at the amine nitrogen ($\angle\text{HOCC}$, $\angle\text{OCCN}$), these angles are described as cis (c, for angles between $0-45^\circ$), gauche (g, $45-135^\circ$), or trans (t, $135-180^\circ$). For salt-bridge conformations [CO_2^-], the proton traditionally on the carboxylic acid is attached to the amine nitrogen and the first dihedral angle is measured from the analogous proton on NH_2 .

Gibbs energies for the cationized glycine complexes at 0 and 298 K, which account for ZPE and thermal corrections, relative to the calculated global minimum (GM) were calculated at four or five levels of theory: three density functional theory (DFT) approaches (B3LYP, B3LYP-GD3BJ, and B3P86), MP2, and in select cases, CCSD(T,full). Relative energies of these conformers, including ZPE corrections and thermal corrections to 298 K with respect to the ground state can be found in Table 1. Table S1 contains the relative energies calculated at 0 K. Ions produced in both instruments at the FELIX Laboratory are believed to have a Maxwell-Boltzmann distribution of energy near room temperature, so the values at 298 K are thought to be more relevant to this discussion. Trends in relative Gibbs energies at 298 K calculated at MP2 for the lowest six conformers are shown in Figure 3. These trends are qualitatively similar to those observed at the B3LYP, B3LYP-GD3BJ, and B3P86 levels of theory, which are shown in the Supporting Information, Figure S2.

All explored levels of theory agree that the GMs for $\text{Li}^+(\text{Gly})$ and $\text{Na}^+(\text{Gly})$ have the [N,CO]-tt structure, a bidentate charge-solvated complex where the metal ion is bound to the amine nitrogen and the free carbonyl oxygen, Figure 2. [N,CO]-tt is predicted to be the GM at both 0 and 298 K for both complexes. For the lithium species, the next lowest-lying structure (18 – 24 kJ/mol above the GM) is the zwitterionic $[\text{CO}_2^-]$ -cc structure, where the metal cation is bound to both of the oxygens of the carboxylate moiety, and the carboxylic acid hydrogen has migrated to the amine nitrogen, Figure 2. All other structures lie more than 22 kJ/mol above the GM, Table 1.

For $\text{Na}^+(\text{Gly})$, the next lowest-lying conformer according to DFT (3 – 10 kJ/mol higher in energy) is the monodentate [CO]-cc structure, where the metal cation binds to the carbonyl oxygen and the carboxylic OH hydrogen bonds to the amine nitrogen, Figure 2. About 2 kJ/mol higher, DFT predicts the bidentate [CO,OH]-cc species, where the metal cation has rotated to interact with the hydroxyl oxygen. The $[\text{CO}_2^-]$ -cc zwitterionic structure lies another 1 – 2 kJ/mol above [CO,OH]-cc according to DFT (7 – 13 kJ/mol above the [N,CO]-tt GM). MP2 predicts a different ordering of these three excited structures, with [CO,OH]-cc lying 7.6 kJ/mol above the GM,

[CO₂]⁻-cc nearly isoenergetic, and [CO]-cc another 1 kJ/mol higher in energy. All other structures lie more than 21 kJ/mol above the GM at all levels of theory.

For K⁺(Gly), theory predicts global minima of either [CO]-cc (DFT) or [CO,OH]-cc (MP2) binding motifs, with the alternative structure within about 2 kJ/mol. The [N,CO]-tt structure is predicted to be 3 – 9 kJ/mol higher in energy than the GM and all other structures are at least 13 kJ/mol above the GM. For the Rb⁺(Gly) and Cs⁺(Gly) complexes, all levels of theory predict the GM to be [CO]-cc at 298 K. At the B3LYP/def2TZVP level of theory, the [CO,OH]-cc structure collapses to [CO]-cc, whereas both B3LYP-GD3BJ and MP2 levels of theory find a potential well for the [CO,OH]-cc structure. The relationship between these structures at the different levels of theory are shown in Figure 4 for K⁺(Gly) and Cs⁺(Gly), which are qualitatively similar to those for Na⁺(Gly) and Rb⁺(Gly), respectively. Figure S3 shows the double-well potentials for all five metal cation complexes (including addition of zero-point energies for stationary states). All other structures of Rb⁺(Gly) and Cs⁺(Gly) are at least 8 kJ/mol above the GM, Table 1.

Comparison of Experimental and Theoretical IR Spectra: Li⁺(Gly)

Figure 5 shows the experimental IRMPD action spectrum along with the theoretical IR spectra of the five lowest-energy structures for the Li⁺(Gly) complex. Experimental bands are found at 666, 864, 992, 1072, 1162, 1285, 1438, 1596, and 1710 cm⁻¹. Theoretical IR spectra are calculated using Gaussian16, which assumes a single photon absorption whereas IRMPD spectra are the result of multiple photons being absorbed. This discrepancy can lead to differences in the intensities of different bands. With this in mind, the calculated spectrum of [N,CO]-tt is in excellent agreement with the IRMPD spectrum. All bands are present and are located at comparable frequencies.

The most intense and highest-frequency experimental band is observed at 1710 cm⁻¹ and corresponds to the CO stretch, predicted to appear at 1701 cm⁻¹ for the [N,CO]-tt conformer. Similar carbonyl stretches are found in all conformers explored, but only those for [N,CO]-tt and [CO]-cc match the experimental band well, see Figure 5. Less intense peaks at 666, 992, 1072, 1162, and 1438 cm⁻¹ are well characterized by the [N,CO]-tt spectrum, and are the most diagnostic

bands predicted by theory. At the B3LYP/6-311+G(d,p) level, the predicted spectrum for [N,CO]-tt has peaks at 666 and 675 cm^{-1} (mainly out-of-plane OH bend and Li-O stretch/NCCO bend); 997 (CN stretch); 1085 cm^{-1} (NH_2 wag); 1175 cm^{-1} (in-plane OH bend); 1413 (CH_2 bend) and 1437 cm^{-1} (CH_2 wag). A minor experimental band observed at 864 cm^{-1} is also reproduced in the [N,CO]-tt spectrum at 841 cm^{-1} (CC stretch and COH bend). The peak observed at 1596 cm^{-1} is shifted in the [N,CO]-tt spectrum to 1628 cm^{-1} (NH_2 bend). A comparable shift in this band has been observed previously in other IRMPD experiments of metalated amino acids and is believed to be a result of strong anharmonic effects.^{2-19, 21} The major discrepancy observed between experiment and the [N,CO]-tt spectrum is the band at 1285 cm^{-1} , whereas the theoretical spectrum shows smaller intensity shifted to 1306 and 1319 cm^{-1} (mainly coupled CH and OH bends). The [N,CO]-ct spectrum is the only one that reproduces this experimental band well, but it does not reproduce the 666, 1438, and 1710 cm^{-1} bands as well as [N,CO]-tt. The high energy of this species also suggests that it is unlikely to contribute to the experimental spectrum. The zwitterionic $[\text{CO}_2^-]$ -cc, monodentate [CO]-cc, and bidentate [CO,OH]-cc binding motifs are also high in energy and do not recreate the spectrum well. Overall, we conclude that the $\text{Li}^+(\text{Gly})$ complex has the [N,CO]tt GM structure.

Comparison of Experimental and Theoretical IR Spectra: $\text{Na}^+(\text{Gly})$

We have previously published a comprehensive examination of the IRMPD spectrum for $\text{Na}^+(\text{Gly})$,²¹ where our spectrum reproduced the much earlier work of Kapota et al.,¹ but was more extensive. There we concluded that the experimental spectrum was reproduced well by the [N,CO]-tt GM structure (similar to the $\text{Li}^+(\text{Gly})$ complex), although predicted intensities in the 1200 – 1500 cm^{-1} region were somewhat low. Peak assignments parallel those made above for $\text{Li}^+(\text{Gly})$. From a spectroscopic point of view, we concluded that minor contributions from the [CO]cc, $[\text{CO}_2^-]$ -cc, and [CO,OH]-cc could be present. This observation is probably consistent with a calculated Maxwell-Boltzmann distribution at 298 K, which suggests that [N,CO]-tt should have

a population of ~90%, with the [CO]-cc, [CO₂]⁻-cc, and [CO,OH]-cc isomers accounting for the remaining 10% in comparable amounts.

Comparison of Experimental and Theoretical IR Spectra: K⁺(Gly)

Figure 6 shows the IRMPD spectrum of K⁺(Gly) compared to the five lowest-lying conformers predicted by theory. The experimental spectrum exhibits bands at 828, 892, 1154, 1330 – 1420, and 1736 cm⁻¹. The carbonyl stretch at 1736 cm⁻¹ is reproduced well in the [CO]-cc, [CO,OH]-cc, and [N,CO]-tt spectra, but not by [CO₂]⁻-cc or [N,CO]-ct. Clearly, the [CO]-cc and [CO,OH]-cc spectra are very similar with small shifts in the CO stretch (1730 and 1750 cm⁻¹, respectively) and in-plane COH bend (1413 and 1387 cm⁻¹, respectively). These shifts could help account for the breadth of the band between 1330 and 1420 cm⁻¹. The bands at 828 and 892 cm⁻¹ are reproduced in both the [CO]-cc and [CO,OH]-cc spectra by bands predicted at 819 and 822 cm⁻¹ (NH₂ wag and CC stretch) and 896 and 899 cm⁻¹ (also NH₂ wag and CC stretch), but the predicted 952 and 948 cm⁻¹ bands (out-of-plane OH bend) are not evident. Neither are bands at 1627 and 1628 cm⁻¹ (NH₂ bend), which is typically red-shifted, as discussed above. The small band observed at 1154 cm⁻¹ can be attributed to a peak predicted for [CO,OH]-cc at 1185 cm⁻¹ (in-plane COH bend and C-OH stretch), which is shifted to 1229 cm⁻¹ in the [CO]-cc spectrum. This band could potentially be assigned to the [N,CO]-tt spectrum, which shows a moderately intense band at 1161 cm⁻¹ (in-plane COH bend), but no evidence for its bands at 997 (NH₂ wag), 633 (OCO bend), and 666 (out-of-plane COH bend) cm⁻¹ are observed. We conclude that the K⁺(Gly) spectrum is consistent with either the [CO]-cc or [CO,OH]-cc spectrum or both.

At this point, it is profitable to again consider the coupling between these two structures, shown in Figure 4, as we have discussed in detail previously (although there, only the B3LYP potential had been calculated).²⁷ Because of this double-well potential, associated with swinging the metal cation around the carbonyl oxygen, the vibrational wavefunctions of this system essentially occupy both structures simultaneously. Whether [CO]-cc or [CO,OH]-cc is the dominant structure depends on the level of theory, with DFT approaches favoring [CO]-cc and MP2 and CCSD(T,full) preferring the [CO,OH]-cc structure. The spectroscopic evidence provided

here is not completely unambiguous, although the appearance of the band at 1154 cm^{-1} is potentially consistent with more population of the $[\text{CO,OH}]\text{-cc}$ structure. According to a Maxwell-Boltzmann distribution at 298 K, the DFT approaches predict 53 – 57% $[\text{CO}]\text{-cc}$, 32 – 43% $[\text{CO,OH}]\text{-cc}$, and 1 – 14% $[\text{N,CO}]\text{-tt}$, whereas MP2 (CCSD(T,full)) indicate populations of 27 (29), 65 (59), and 8 (12)%, respectively. Thus, the MP2 relative energies tend to agree better with the observed spectrum and with CCSD(T) calculations.

One can also wonder whether the double-well potential might influence the harmonic frequency calculations as the proximity of the coupled potential wells clearly changes the how quadratic the potential is. To test this, we also performed anharmonic frequency calculations, which are shown in Figure 7. The anharmonic $[\text{CO,OH}]\text{-cc}$ predictions (including overtones and combination bands) at the B3LYP/6-311+G(d,p) level (no scaling) agree very well with the experimental spectrum, reproducing the bands at 892, 1154, 1330 – 1420, and 1736 cm^{-1} . Intense fundamental anharmonic frequencies are predicted at 883 (NH_2 wag and CC stretch), 1163 (in-plane COH bend and C-OH stretch), 1373 (in-plane COH bend), and 1750 cm^{-1} (CO stretch). The shape of the 892 cm^{-1} band, position of the 1154 cm^{-1} band, and width of the 1330 – 1420 cm^{-1} band are better reproduced by the anharmonic $[\text{CO,OH}]\text{-cc}$ spectrum than its harmonic analogue. Agreement between experiment and the anharmonic $[\text{CO}]\text{-cc}$ spectrum is less satisfying, with the CO stretch peak red-shifted (fundamental at 1732 cm^{-1} with combination bands at 1690 and 1710 cm^{-1}), the in-plane COH bend blue-shifted (fundamental at 1394 cm^{-1} and combination bands at 1386 and 1421 cm^{-1}), and no band near 1163 cm^{-1} (shifted to 1206 cm^{-1}). Overall, the anharmonic spectral comparisons suggest that the $[\text{CO,OH}]\text{-cc}$ structure is probably the dominant $\text{K}^+(\text{Gly})$ species present experimentally, with contributions from the $[\text{CO}]\text{-cc}$ structure still possible.

Comparison of Experimental and Theoretical IR Spectra: $\text{Rb}^+(\text{Gly})$ and $\text{Cs}^+(\text{Gly})$

Comparison of the experimental spectra in Figure 1 suggests that the three heavier alkali cations should have similar binding motifs with Gly. Therefore, we focus here on a comparison of the $[\text{CO}]\text{-cc}$ and $[\text{CO,OH}]\text{-cc}$ structures with experiment for both $\text{Rb}^+(\text{Gly})$ and $\text{Cs}^+(\text{Gly})$. Figure

S4, which compares these experimental spectra with theoretical spectra of the five lowest energy structures, confirms that the higher energy species do not reproduce the experimental spectra (although the bands predicted for the related $[\text{CO}_2^-]$ -cc structure are consistent with many of the observed bands). Figures 8 and 9 show the IRMPD spectra of $\text{Rb}^+(\text{Gly})$ and $\text{Cs}^+(\text{Gly})$ compared to spectra of the $[\text{CO}]$ -cc and $[\text{CO},\text{OH}]$ -cc structures predicted by theory for both scaled harmonic and unscaled anharmonic (including overtones and combination bands) frequencies. The $[\text{CO}]$ -cc calculations were performed at the B3LYP/def2TZVP level, whereas the $[\text{CO},\text{OH}]$ -cc calculations utilized MP2/def2TZVP level of theory because the B3LYP approach collapses to $[\text{CO}]$ -cc, see Figures 4 and S3. As for $\text{K}^+(\text{Gly})$, the distinctions between the harmonic and anharmonic calculations are small with the only major difference being the red-shift in the minor bands near 1620 cm^{-1} in all harmonic spectra (NH_2 bend).

The experimental spectrum of $\text{Rb}^+(\text{Gly})$ exhibits bands at 752, 886, 926, 1075, 1141, 1389, 1591, and 1726 cm^{-1} . The carbonyl stretch at 1726 cm^{-1} is reproduced well in the $[\text{CO}]$ -cc spectrum (harmonic/anharmonic: $1735/1738\text{ cm}^{-1}$), whereas the $[\text{CO},\text{OH}]$ -cc peaks are blue-shifted ($1771/1775\text{ cm}^{-1}$). The band observed at 1591 cm^{-1} can plausibly be assigned to the NH_2 bend of either $[\text{CO}]$ -cc ($1627/1561$ -combination band cm^{-1}) or $[\text{CO},\text{OH}]$ -cc ($1627/1603\text{ cm}^{-1}$). The in-plane COH bend at 1389 cm^{-1} is reproduced best by the anharmonic $[\text{CO}]$ -cc species (1380 cm^{-1}) with a combination band at 1394 cm^{-1} also contributing. The analogous peaks in the other three spectra are blue-shifted slightly. The anharmonic $[\text{CO}]$ -cc spectrum also reproduces the bands in the $750 - 950\text{ cm}^{-1}$ region fairly well, with predicted intensity at 798, 873 (both NH_2 wag and CC stretch), and 918 (combination band) cm^{-1} . In this region, the $[\text{CO}]$ -cc spectra are clearly more accurate than the $[\text{CO},\text{OH}]$ -cc spectra, which have a peak near 1000 cm^{-1} that is not observed. As for $\text{K}^+(\text{Gly})$, the minor peak observed 1141 cm^{-1} could be affiliated with $[\text{CO},\text{OH}]$ -cc structure, in-plane COH bend at the $1206/1182\text{ cm}^{-1}$, but it may also be explained by the anharmonic spectrum of $[\text{CO}]$ -cc, which shifts the comparable band from 1222 cm^{-1} in the harmonic spectrum to 1200 cm^{-1} in the anharmonic spectrum while doubling its intensity. This spectrum also predicts a weak band at 1053 cm^{-1} (CN stretch), which could correspond to the band observed at 1075 cm^{-1} . This

comparison also suggests that the $\text{Rb}^+(\text{Gly})$ spectrum may be saturated, thereby overemphasizing the minor bands and suppressing those at 1389 and 1726 cm^{-1} . This hypothesis is consistent with the observation that this complex exhibited the highest extent of dissociation among those studied here and with the comparison with the ion trap experiment, Figure S1. Overall, the observed spectrum seems most consistent with the $[\text{CO}]\text{-cc}$ structure, which is predicted to be the 298 K GM at all levels of theory, although contributions from the $[\text{CO,OH}]\text{-cc}$ structure cannot be eliminated nor could minor contributions from the much higher energy $[\text{CO}_2]\text{-cc}$ species.

The analysis of the $\text{Cs}^+(\text{Gly})$ results closely parallels that for $\text{Rb}^+(\text{Gly})$, see Figure 9. Again, the anharmonic spectrum of the $[\text{CO}]\text{-cc}$ GM provides a very good reproduction of the experimental spectrum. All bands can be assigned analogously with the $\text{Rb}^+(\text{Gly})$ discussion above. We again conclude that the dominant experimental structure is $[\text{CO}]\text{-cc}$, the 298 K GM at all levels of theory.

The dominance of the $[\text{CO}]\text{-cc}$ structure for both $\text{Rb}^+(\text{Gly})$ and $\text{Cs}^+(\text{Gly})$ is clearly consistent with the B3LYP and B3LYP-GD3BJ potentials shown in Figures S3 and 4 but appears to be at odds with the MP2 potentials, even though MP2 and CCSD(T,full) calculations predict $[\text{CO}]\text{-cc}$ is the GM at 298 K , Table 1. To understand the dichotomy, it can be realized that the potentials shown do not include zero-point energies (ZPE) nor enthalpic and entropic thermal corrections. Indeed, the ZPEs for $[\text{CO,OH}]\text{-cc}$ are larger than those for $[\text{CO}]\text{-cc}$ by 1.6_3 and 1.6_7 kJ/mol for $\text{Rb}^+(\text{Gly})$ and $\text{Cs}^+(\text{Gly})$, respectively, thus destabilizing $[\text{CO,OH}]\text{-cc}$ relative to $[\text{CO}]\text{-cc}$. (Figure S3 shows these 0 K relative energies for the stationary states.) The 298 K thermal corrections (including ZPE) are even larger: 4.0 and 4.4 kJ/mol, largely because the metal ion is able to move more freely in the monodentate $[\text{CO}]\text{-cc}$ than in the bidentate $[\text{CO,OH}]\text{-cc}$. When these energies are included in the potentials shown in Figures S3 and 4, the complexes lie well above the barrier between the two structures. Thus, the system spends more time in the entropically favored $[\text{CO}]\text{-cc}$ structure, no matter whether the surface looks like that calculated at the DFT levels or the MP2 level.

Conclusion

IRMPD spectra of the five alkali metal cations coordinated with the simplest amino acid, glycine, are acquired. Comparison of these spectra to calculated spectra demonstrate that the $\text{Li}^+(\text{Gly})$ and $\text{Na}^+(\text{Gly})$ complexes have $[\text{N},\text{CO}]\text{-tt}$ structures, although minor contributions of $[\text{CO}]\text{-cc}$, $[\text{CO},\text{OH}]\text{-cc}$, and $[\text{CO}_2^-]\text{-cc}$ are likely for the latter complex. For the three heavier metal complexes, $\text{K}^+(\text{Gly})$, $\text{Rb}^+(\text{Gly})$, and $\text{Cs}^+(\text{Gly})$, the spectra are reproduced by $[\text{CO},\text{OH}]\text{-cc}$ and $[\text{CO}]\text{-cc}$ structures, with the former favored for the K complex and the latter for the Rb and Cs complexes. These results are generally in good agreement with predictions of the global minimum structures at all levels of theory considered, but there is some evidence that MP2 relative Gibbs energies at 298 K are more consistent with the data than DFT Gibbs energies and the former also agree better with limited CCSD(T,full) results as well, Table 1. The contribution of the double-well potential that links the $[\text{CO},\text{OH}]\text{-cc}$ and $[\text{CO}]\text{-cc}$ structures is considered in some detail. Anharmonic calculations that should include at least some aspects of this coupling provide better reproductions of the spectroscopic data than scaled harmonic calculations.

Supporting Information

Table S1 provides relative Gibbs energies at 0 K for various structures of $\text{M}^+(\text{Gly})$, $\text{M}^+ = \text{Li}^+, \text{Na}^+, \text{K}^+, \text{Rb}^+, \text{and } \text{Cs}^+$, calculated at five levels of theory. Figure S1 compares IRMPD spectra taken on the QIT and FTICR. Figure S2 shows relative energies of the five lowest energy structures of $\text{M}^+(\text{Gly})$ calculated at four levels of theory. Figure S3 compares the relaxed potential energy surfaces for changing the MOC bond angle in $\text{M}^+(\text{Gly})$ for $\text{M}^+ = \text{Li}^+, \text{Na}^+, \text{K}^+, \text{Rb}^+, \text{and } \text{Cs}^+$ calculated at three levels of theory. Figure S4 compares experimental IRMPD spectra for $\text{Rb}^+(\text{Gly})$ and $\text{Cs}^+(\text{Gly})$ to harmonic frequency calculations for the lowest five structures at the B3LYP/def2TZVP level.

Conflicts of Interest

There are no conflicts of interest to declare.

Acknowledgement

Financial support for this work was provided by the National Science Foundation (Grant CHE-1954142). The authors gratefully acknowledge the *Nederlandse Organisatie voor Wetenschappelijk Onderzoek* (NWO) for the support of the FELIX Laboratory. In addition, the authors thank the Center for High-Performance Computing at the University of Utah for generous allocation of computer time.

References

1. Kapota, C.; Lemaire, J.; Maitre, P.; Ohanessian, G., Vibrational Signature of Charge Solvation vs Salt Bridge Isomers of Sodiated Amino Acids in the Gas Phase. *J. Am. Chem. Soc.* **2004**, *126*, 1836-1842.
2. Polfer, N. C.; Oomens, J.; Dunbar, R. C., IRMPD Spectroscopy of Metal-Ion/Tryptophan Complexes. *Phys. Chem. Chem. Phys.* **2006**, *8*, 2744-2751.
3. Dunbar, R. C.; Polfer, N. C.; Oomens, J., Gas-phase zwitterion stabilization by a metal dication. *J. Am. Chem. Soc.* **2007**, *129*, 14562-14563.
4. Forbes, M. W.; Bush, M. F.; Polfer, N. C.; Oomens, J.; Dunbar, R. C.; Williams, E. R.; Jockusch, R. A., Infrared Spectroscopy of Arginine Cation Complexes: Direct Observation of Gas-Phase Zwitterions. *J. Phys. Chem. A* **2007**, *111*, 11759-11770.
5. Bush, M. F.; Forbes, M. W.; Jockusch, R. A.; Oomens, J.; Polfer, N. C.; Saykally, R. J.; Williams, E. R., Infrared Spectroscopy of Cationized Lysine and ϵ -N-methyllysine in the Gas Phase: Effects of Alkali-Metal Ion Size and Proton Affinity on Zwitterion Stability. *J. Phys. Chem. A* **2007**, *111* (32), 7753-7760.
6. Bush, M. F.; O'Brien, J. T.; Prell, J. S.; Saykally, R. J.; Williams, E. R., Infrared Spectroscopy of Cationized Arginine in the Gas Phase: Direct Evidence for the Transition from Nonzwitterionic to Zwitterionic Structure. *J. Am. Chem. Soc.* **2007**, *129*, 1612-1622.
7. Drayss, M. K.; Blunk, D.; Oomens, J.; Schäfer, M., Infrared Multiple Photon Dissociation Spectroscopy of Potassiated Proline. *J. Phys. Chem. A* **2008**, *112*, 11972-11974.
8. Bush, M. F.; Oomens, J.; Saykally, R. J.; Williams, E. R., Effects of Alkaline Earth Metal Ion Complexation on Amino Acid Zwitterion Stability: Results from Infrared Action Spectroscopy. *J. Am. Chem. Soc.* **2008**, *130*, 6463-6471.
9. Bush, M. F.; Oomens, J.; Saykally, R. J.; Williams, E. R., Alkali Metal Ion Binding to Glutamine and Glutamine Derivatives Investigated by Infrared Action Spectroscopy and Theory. *J. Phys. Chem. A* **2008**, *112*, 8578-8584.
10. O'Brien, J. T.; Prell, J. S.; Steill, J. D.; Oomens, J.; Williams, E. R., Interactions of Mono- and Divalent Metal Ions with Aspartic and Glutamic Acid Investigated with IR Photodissociation Spectroscopy and Theory. *J. Phys. Chem. A* **2008**, *112*, 10823-10830.
11. Rodgers, M. T.; Armentrout, P. B.; Oomens, J.; Steill, J. D., Infrared Multiphoton Dissociation Spectroscopy of Cationized Threonine: Effects of Alkali-Metal Cation Size on Gas-Phase Conformation. *J. Phys. Chem. A* **2008**, *112*, 2258-2267.

12. Armentrout, P. B.; Rodgers, M. T.; Oomens, J.; Steill, J. D., Infrared Multiphoton Dissociation Spectroscopy of Cationized Serine: Effects of Alkali-Metal Cation Size on Gas-Phase Conformation. *J. Phys. Chem. A* **2008**, *112*, 2248-2257.
13. Bush, M. F.; Oomens, J.; Williams, E. R., Proton Affinity and Zwitterion Stability: New Results from Infrared Spectroscopy and Theory of Cationized Lysine and Analogues in the Gas Phase. *J. Phys. Chem. A* **2009**, *113*, 431-438.
14. Heaton, A. L.; Bowman, V. N.; Oomens, J.; Steill, J. D.; Armentrout, P. B., Infrared Multiple Photon Dissociation Spectroscopy of Cationized Asparagine: Effects of Metal Cation Size on Gas-Phase Conformation. *J. Phys. Chem. A* **2009**, *113* (19), 5519-5530.
15. Dunbar, R. C.; Steill, J. D.; Oomens, J., Cationized phenylalanine conformations characterized by IRMPD and computation for singly and doubly charged ions. *Phys. Chem. Chem. Phys.* **2010**, *12* (41), 13383-13393.
16. Carl, D. R.; Cooper, T. E.; Oomens, J.; Steill, J. D.; Armentrout, P. B., Infrared Multiple Photon Dissociation Spectroscopy of Cationized Methionine: Effects of Alkali-Metal Cation Size on Gas-Phase Conformation. *Phys. Chem. Chem. Phys.* **2010**, *12*, 3384-3398.
17. Citir, M.; Stennett, E. M. S.; Oomens, J.; Steill, J. D.; Rodgers, M. T.; Armentrout, P. B., Infrared Multiple Photon Dissociation Spectroscopy of Cationized Cysteine: Effects of Metal Cation Size on Gas-Phase Conformation. *Int. J. Mass Spectrom.* **2010**, *297*, 9-17.
18. Drayss, M. K.; Armentrout, P. B.; Oomens, J.; Schäfer, M., IR Spectroscopy of Cationized Aliphatic Amino Acids: Stability of Charge-solvated Structure Increases with Metal Cation Size. *Int. J. Mass Spectrom.* **2010**, *297*, 18-27.
19. Citir, M.; Hinton, C. S.; Oomens, J.; Steill, J. D.; Armentrout, P. B., Infrared Multiple Photon Dissociation Spectroscopy of Cationized Histidine: Effects of Metal Cation Size on Gas-Phase Conformation. *J. Phys. Chem. A* **2012**, *116*, 1532-1541.
20. Feng, R.; Xu, Y.; Kong, X., Structural Diversity of Di-Metalized Arginine Evidenced by Infrared Multiple Photon Dissociation (IRMPD) Spectroscopy in the Gas Phase. *Molecules* **2021**, *26* (21), 6546.
21. Armentrout, P. B.; Boles, G. C.; Ghassee, M.; Berden, G.; Oomens, J., Infrared Multiple-Photon Dissociation Spectra of Sodiated Complexes of the Aliphatic Amino Acids. *J. Phys. Chem. A* **2021**, *125* (29), 6348-6355.
22. Moision, R. M.; Armentrout, P. B., An Experimental and Theoretical Dissection of Sodium Cation/Glycine Interactions. *J. Phys. Chem. A* **2002**, *106*, 10350-10362.
23. Moision, R. M.; Armentrout, P. B., An Experimental and Theoretical Dissection of Potassium Cation/Glycine Interactions. *Phys. Chem. Chem. Phys.* **2004**, *6*, 2588-2599.
24. Bowman, V. N.; Heaton, A. L.; Armentrout, P. B., Metal Cation Dependence of Interactions with Amino Acids: Bond Energies of Rb⁺ to Gly, Ser, Thr, and Pro. *J. Phys. Chem. B* **2010**, *114*, 4107-4114.
25. Armentrout, P. B.; Chen, Y.; Rodgers, M. T., Metal Cation Dependence of Interactions with Amino Acids: Bond Energies of Cs⁺ to Gly, Pro, Ser, Thr, and Cys. *J. Phys. Chem. A* **2012**, *116* (16), 3989-3999.
26. Rodgers, M. T.; Armentrout, P. B., A Critical Evaluation of the Experimental and Theoretical Determination of Lithium Cation Affinities. *Int. J. Mass Spectrom.* **2007**, *267*, 167-182.
27. Jones, R. M.; Nilsson, T.; Walker, S.; Armentrout, P. B., Potassium Binding Interactions with the Aliphatic Amino Acids: Thermodynamic and Entropic Effects Analyzed via a Guided Ion Beam and Computational Study. *J. Am. Soc. Mass. Spectrom.* **2022**, in press.

28. Valle, J. J.; Eyler, J. R.; Oomens, J.; Moore, D. T.; van der Meer, A. F. G.; von Helden, G.; Meijer, G.; Hendrickson, C. L.; Marshall, A. G.; Blakney, G. T., Free Electron Laser-Fourier Transform Ion Cyclotron Resonance Mass Spectrometry Facility for Obtaining Infrared Multiphoton Dissociation Spectra of Gaseous Ions. *Rev. Sci. Instrum.* **2005**, *76*, 023103.
29. Polfer, N. C.; Oomens, J., Reaction products in mass spectrometry elucidated with infrared spectroscopy. *Phys. Chem. Chem. Phys.* **2007**, *9*, 3804-3817.
30. Polfer, N. C.; Oomens, J.; Moore, D. T.; von Helden, G.; Meijer, G.; Dunbar, R. C., Infrared Spectroscopy of Phenylalanine Ag(I) and Zn(II) Complexes in the Gas Phase. *J. Am. Chem. Soc.* **2006**, *128*, 517-525.
31. Oepts, D.; van der Meer, A. F. G.; van Amersfoort, P. W., The Free-Electron-Laser User Facility FELIX. *Infrared Phys. Technol.* **1995**, *36*, 297-308.
32. Lemaire, J.; Boissel, P.; Heninger, M.; Mauclair, G.; Bellec, G.; Mestdagh, H.; Le Caer, S.; Ortega, J.; Glotin, F.; Maître, P., Gas Phase Infrared Spectroscopy of Selectively Prepared Ions. *Phys. Rev. Lett.* **2002**, *89*, 273002.
33. Berden, G.; Derksen, M.; Houthuijs, K. J.; Martens, J.; Oomens, J., An Automatic Variable Laser Attenuator for IRMPD Spectroscopy and Analysis of Power-dependence in Fragmentation Spectra. *Int. J. Mass Spectrom.* **2019**, *443*, 1-8.
34. Frisch, M. J.; Trucks, G. W.; Schlegel, H. B.; Scuseria, G. E.; Robb, M. A.; Cheeseman, J. R.; Scalmani, G.; Barone, V.; Petersson, G. A.; Nakatsuji, H.; Li, X.; Caricato, M.; Marenich, A. V.; Bloino, J.; Janesko, B. G.; Gomperts, R.; Mennucci, B.; Hratchian, H. P.; Ortiz, J. V.; Izmaylov, A. F.; Sonnenberg, J. L.; Williams-Young, D.; Ding, F.; Lipparini, F.; Egidi, F.; Goings, J.; Peng, B.; Petrone, A.; Henderson, T.; Ranasinghe, D.; Zakrzewski, V. G.; Gao, J.; Rega, N.; Zheng, G.; Liang, W.; Hada, M.; Ehara, M.; Toyota, K.; Fukuda, R.; Hasegawa, J.; Ishida, M.; Nakajima, T.; Honda, Y.; Kitao, O.; Nakai, H.; Vreven, T.; Throssell, K.; J. A. Montgomery, J.; Peralta, J. E.; Ogliaro, F.; Bearpark, M. J.; Heyd, J. J.; Brothers, E. N.; Kudin, K. N.; Staroverov, V. N.; Keith, T. A.; Kobayashi, R.; Normand, J.; Raghavachari, K.; Rendell, A. P.; Burant, J. C.; Iyengar, S. S.; Tomasi, J.; Cossi, M.; Millam, J. M.; Klene, M.; Adamo, C.; Cammi, R.; Ochterski, J. W.; Martin, R. L.; Morokuma, K.; Farkas, O.; Foresman, J. B.; Fox, D. *J. Gaussian 16, Revision A.03*, Gaussian, Inc.: Wallingford CT, 2016.
35. Becke, A. D., Density-functional Thermochemistry. III. The Role of Exact Exchange. *J. Chem. Phys.* **1993**, *98*, 5648-5652.
36. Ditchfield, R.; Hehre, W. J.; Pople, J. A., Self-Consistent Molecular-Orbital Methods. IX. An Extended Gaussian-Type Basis for Molecular-Orbital Studies of Organic Molecules. *J. Chem. Phys.* **1971**, *54*, 724-728.
37. McLean, A. D.; Chandler, G. S., Contracted Gaussian Basis Sets for Molecular Calculations. I. Second Row Atoms, Z=11-18. *J. Chem. Phys.* **1980**, *72*, 5639-5648.
38. Krishnan, R.; Binkley, J. S.; Seeger, R.; Pople, J. A., Self-consistent Molecular Orbital Methods. XX. A Basis Set for Correlated Wave Functions. *J. Chem. Phys.* **1980**, *72*, 650-654.
39. Feller, D., The Role of Databases in Support of Computational Chemistry Calculations. *J. Comput. Chem.* **1996**, *17* (13), 1571-1586.
40. Grimme, S.; Ehrlich, S.; Goerigk, L., Effect of the Damping Function in Dispersion Corrected Density Functional Theory. *J. Comput. Chem.* **2011**, *32* (7), 1456-1465.
41. Grimme, S.; Antony, J.; Ehrlich, S.; Krieg, H., A Consistent and Accurate Ab Initio Parametrization of Density Functional Dispersion Correction (DFT-D) for the 94 Elements H-Pu. *J. Chem. Phys.* **2010**, *132* (15), 154104-154119.

42. Foresman, J. B.; Frisch, A. E., *Exploring Chemistry with Electronic Structure Methods*. 2nd ed.; Gaussian, Inc.: Pittsburgh, PA, 1996.
43. Bauschlicher, C. W.; Partridge, H., A modification of the Gaussian-2 approach using density functional theory. *J. Chem. Phys.* **1995**, *103* (5), 1788-91.
44. Martens, J.; Berden, G.; Gebhardt, C. R.; Oomens, J., Infrared ion spectroscopy in a modified quadrupole ion trap mass spectrometer at the FELIX free electron laser laboratory. *Rev. Sci. Instrum.* **2016**, *87* (10), 103108.

Table 1: 298 K Relative Gibbs Energies (kJ/mol) of Low-Lying Conformers of $M^+(\text{Gly})$ Calculated at B3LYP, B3LYP-GD3BJ, B3P86, and MP2 Levels of Theory^a

Structure	Li ⁺ (Gly)	Na ⁺ (Gly)	K ⁺ (Gly)	Rb ⁺ (Gly)	Cs ⁺ (Gly)
[N,CO]-tt	0.0, 0.0, 0.0, 0.0	0.0, 0.0, 0.0, 0.0	6.7, 3.3, 9.3, 5.3 (3.9)	11.2, 8.2, 14.1, 7.7	14.7, 11.5, 16.8, 10.6
[CO ₂]-cc	23.0, 24.1, 20.0, 18.5	10.6, 13.4, 7.5, 7.7	15.5, 14.6, 14.3, 12.9	23.8, 23.1, 21.9, 16.7	26.4, 25.3, 23.7, 18.1
[N,CO]-ct	23.8, 22.5, 23.6, 24.2	21.5, 21.2, 21.3, 21.8	26.4, 22.8, 28.9, 25.4	29.9, 26.9, 32.6, 27.4	31.9, 28.8, 34.0, 28.4
[CO]-cc	28.9, 30.2, 25.3, 32.0	7.2, 10.3, 3.0, 8.7	0.0, 0.0, 0.0, 2.2 (1.7)	0.0, 0.0, 0.0, 0.0 (0.0)	0.0, 0.0, 0.0, 0.0 (0.0)
[CO,OH]-cc	42.5, ^b 40.5, ^b 37.0, ^b 39.6 ^b	9.2, 12.1, 5.1, 7.6	0.9, 1.3, 0.6, 0.0 (0.0)	6.9, ^b 1.6, 5.2, ^b 0.6 ^b (1.9)	7.1, ^b 0.9, 5.1, ^b 1.6, ^b (3.0)
[N,OH]-tc	47.6, 44.4, 49.8, 41.2	41.2, 39.2, 42.8, 35.6	44.3, 38.5, 48.2, 37.7	47.5, 42.2, 51.7, 39.7	49.9, 44.4, 53.3, 42.4
[CO]-tc	68.8, 70.5, 69.2, 73.9	44.7, 48.5, 44.2, 47.3	34.0, 34.7, 37.7, 37.1	34.2, 44.2, ^c 38.6, 35.4	32.9, 33.6, 36.9, 35.1
[CO]-ct	70.2, 71.8, 70.3, 75.0	45.2, 48.6, 44.5, 47.8	35.7, 35.9, 39.2, 38.7	35.2, 35.6, 38.6, 38.0	33.9, 34.2, 37.6, 35.9
[N]-tt	85.3, 84.1, 82.7, 80.2	57.3, 58.0, 55.7, 53.3	48.8, 46.3, 51.0, 45.4	47.4, 45.4, 50.0, 43.3	46.2, 43.7, 48.6, 44.6

^a B3LYP, B3LYP-GD3BJ, B3P86, and MP2 (CCSD(T,full)) values calculated using the 6-311+G(2d,2p) for Li, Na, and K or def2TZVPP for Rb and Cs basis sets. B3LYP, B3P86, and MP2 values use structures and zero-point energies calculated at the B3LYP/6-311+G(d,p) or B3LYP/def2TZVP level of theory. B3LYP-GD3BJ values use structures and zero-point energies calculated at the B3LYP-GD3BJ/6-311+G(d,p) or B3LYP-GD3BJ/def2TZVP level of theory. Bold indicates the ground state. ^b Collapses to [CO]-cc at B3LYP and B3LYP-GD3BJ levels. Values are single point calculations using MP2/6-311+G(d,p) or MP2/def2TZVP structures and zero-point energies. ^c Collapses to [N,CO]-tt. Value is single point calculation using B3LYP/def2TZVP structure and zero-point energy.

Figure Captions

Figure 1: Infrared multiple photon dissociation action spectra of $M^+(\text{Gly})$ complexes where $M^+ = \text{Li}^+, \text{Na}^+, \text{K}^+, \text{Rb}^+, \text{and } \text{Cs}^+$ acquired on the FTICR MS.

Figure 2: Structures of $\text{Rb}^+(\text{Gly})$ complexes calculated at the B3LYP/def2TZVP level of theory, except $[\text{CO},\text{OH}]\text{-cc}$ which was an MP2/def2TZVP calculation. Dashed lines show metal-ligand interactions; dotted lines indicate hydrogen bonding interactions. Rb – purple, O – red, N – blue, C – grey, H – white.

Figure 3. Relative Gibbs energies (kJ/mol) at 298 K calculated at the MP2/6-311+G(2d,2p) or MP2/def2TZVPP level of theory for six distinct structures of $M^+(\text{Gly})$, where $M^+ = \text{Li}^+, \text{Na}^+, \text{K}^+, \text{Rb}^+, \text{and } \text{Cs}^+$ as a function of the alkali-metal cation relative to the energy of the most stable structure.

Figure 4: Relaxed potential energy surface scans of the MOC bond angle in $M^+(\text{Gly})$ calculated at the B3LYP, B3LYP-GD3BJ, and MP2 levels of theory for $M = \text{K}$ (6-311+G(d,p) basis set) and $M = \text{Cs}$ (def2TZVP basis set).

Figure 5: Comparison of the experimental IRMPD action spectrum for $\text{Li}^+(\text{Gly})$ (dashed line) with harmonic IR spectra for five structures predicted at the B3LYP/6-311+G(d,p) level of theory. Relative Gibbs energies (kJ/mol) at 298 K are provided at the B3LYP, B3LYP-GD3BJ, B3P86, and MP2 levels.

Figure 6: Comparison of the experimental IRMPD action spectrum for $K^+(\text{Gly})$ (dashed line) with harmonic IR spectra for five structures predicted at the B3LYP/6-311+G(d,p) level of theory. Relative Gibbs energies (kJ/mol) at 298 K are provided at the B3LYP, B3LYP-GD3BJ, B3P86, and MP2 levels.

Figure 7: Comparison of the experimental IRMPD action spectrum for $K^+(\text{Gly})$ (dashed line) with anharmonic IR spectra for two structures predicted at the B3LYP/6-311+G(d,p) level of theory. Relative Gibbs energies (kJ/mol) at 298 K are provided at the B3LYP, B3LYP-GD3BJ, B3P86, and MP2 levels.

Figure 8: Comparison of the experimental IRMPD action spectrum for $Rb^+(\text{Gly})$ (dashed line) with harmonic and anharmonic IR spectra for two structures predicted at the B3LYP/def2TZVP level for [CO]-cc and MP2/def2TZVP level of theory for [CO,OH]-cc. Relative Gibbs energies (kJ/mol) at 298 K are provided at the B3LYP, B3LYP-GD3BJ, B3P86, and MP2 levels.

Figure 9: Comparison of the experimental IRMPD action spectrum for $Rb^+(\text{Gly})$ (dashed line) with harmonic and anharmonic IR spectra for two structures predicted at the B3LYP/def2TZVP level for [CO]-cc and MP2/def2TZVP level of theory for [CO,OH]-cc. Relative Gibbs energies (kJ/mol) at 298 K are provided at the B3LYP, B3LYP-GD3BJ, B3P86, and MP2 levels.

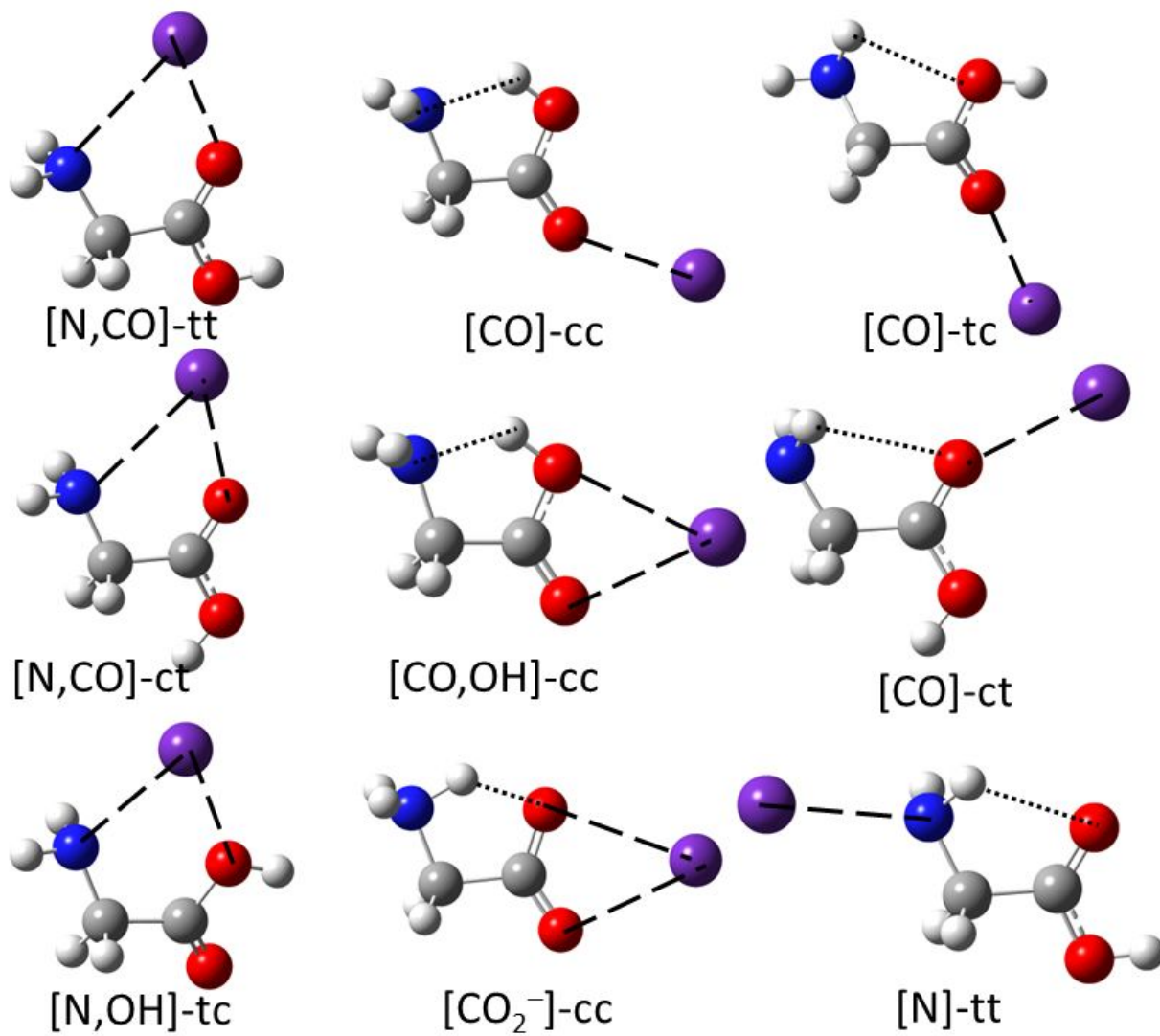


Figure 2

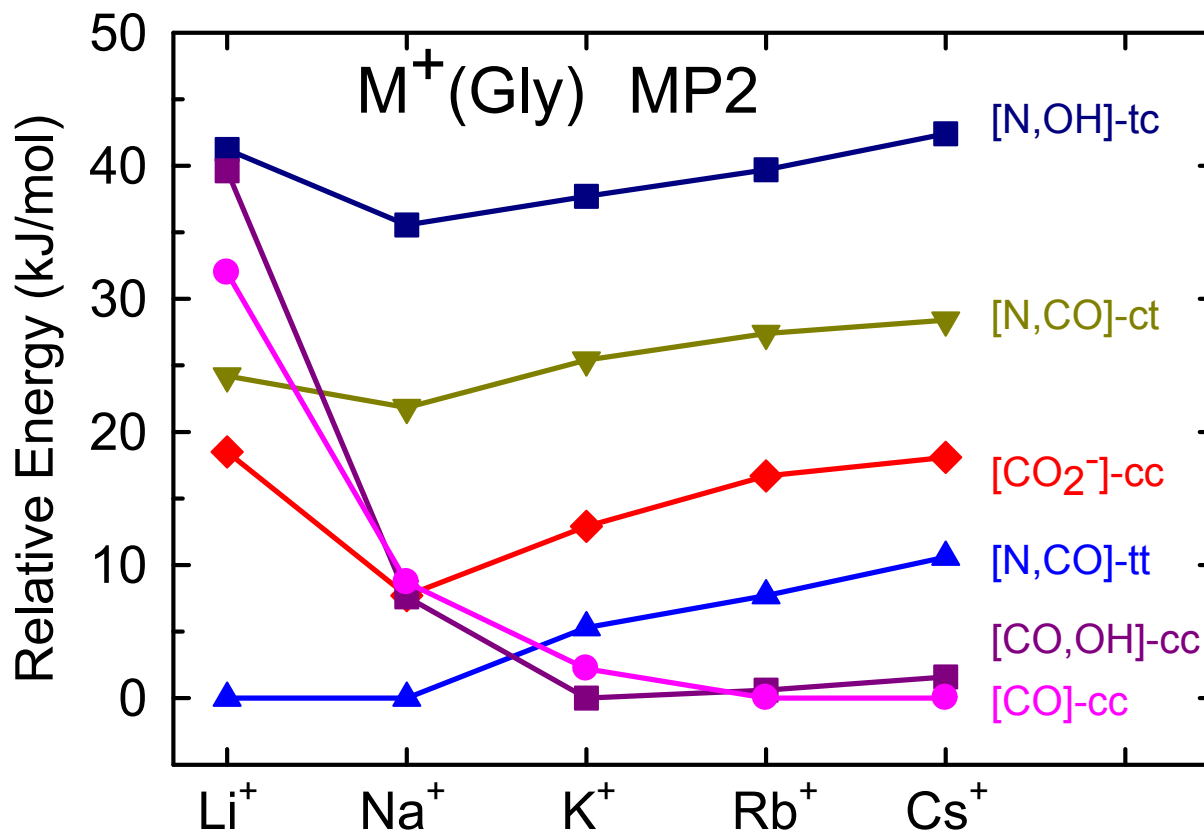


Figure 3

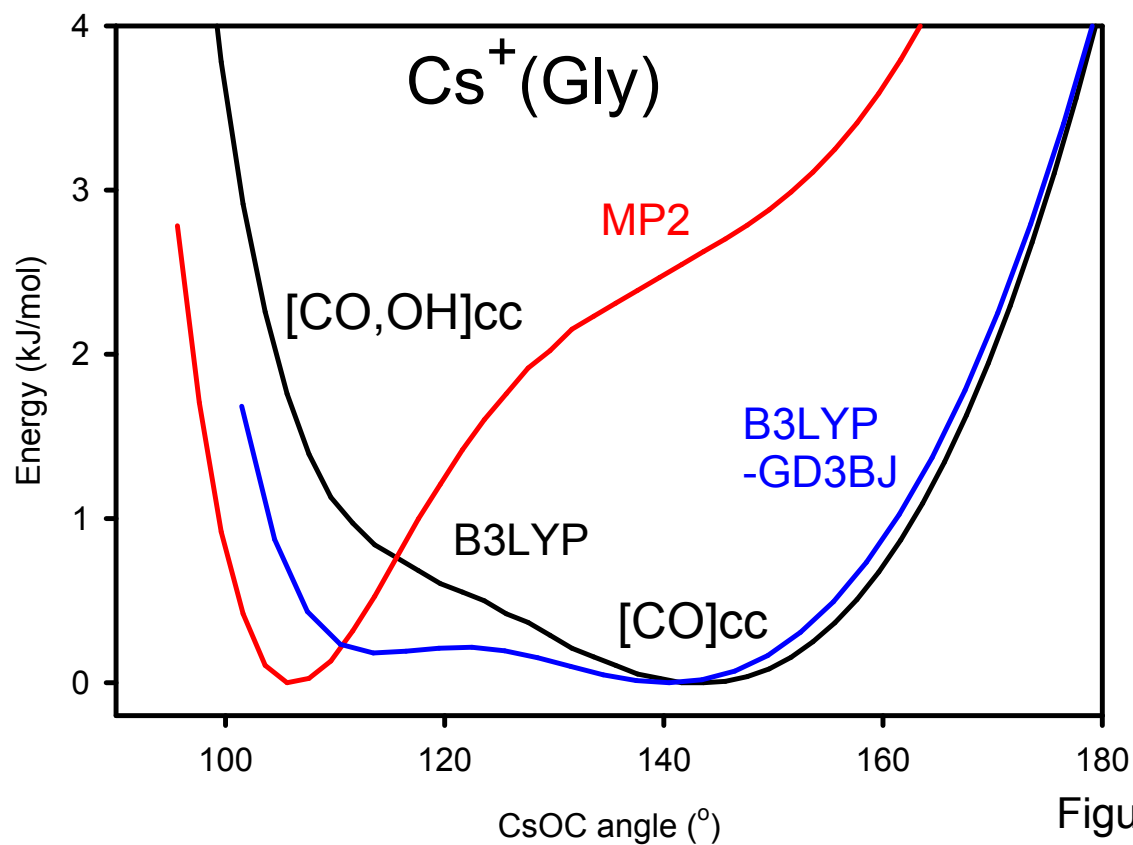
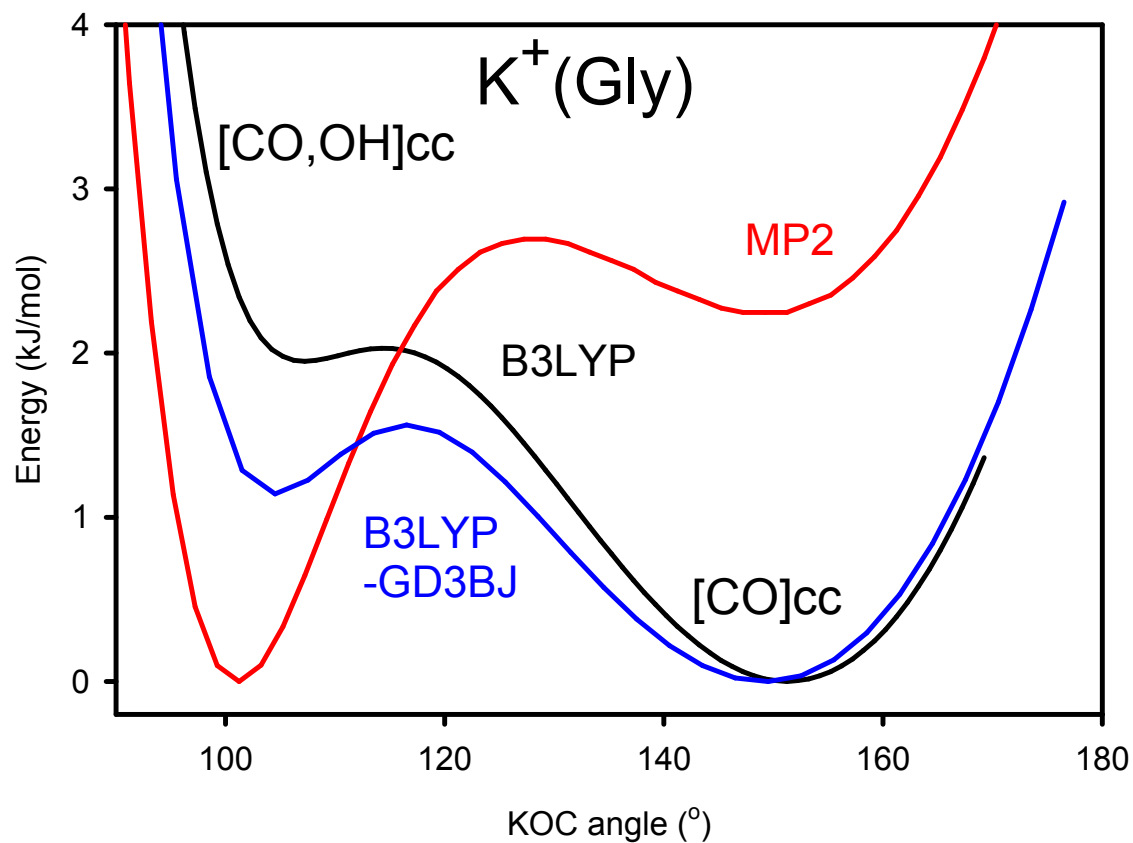
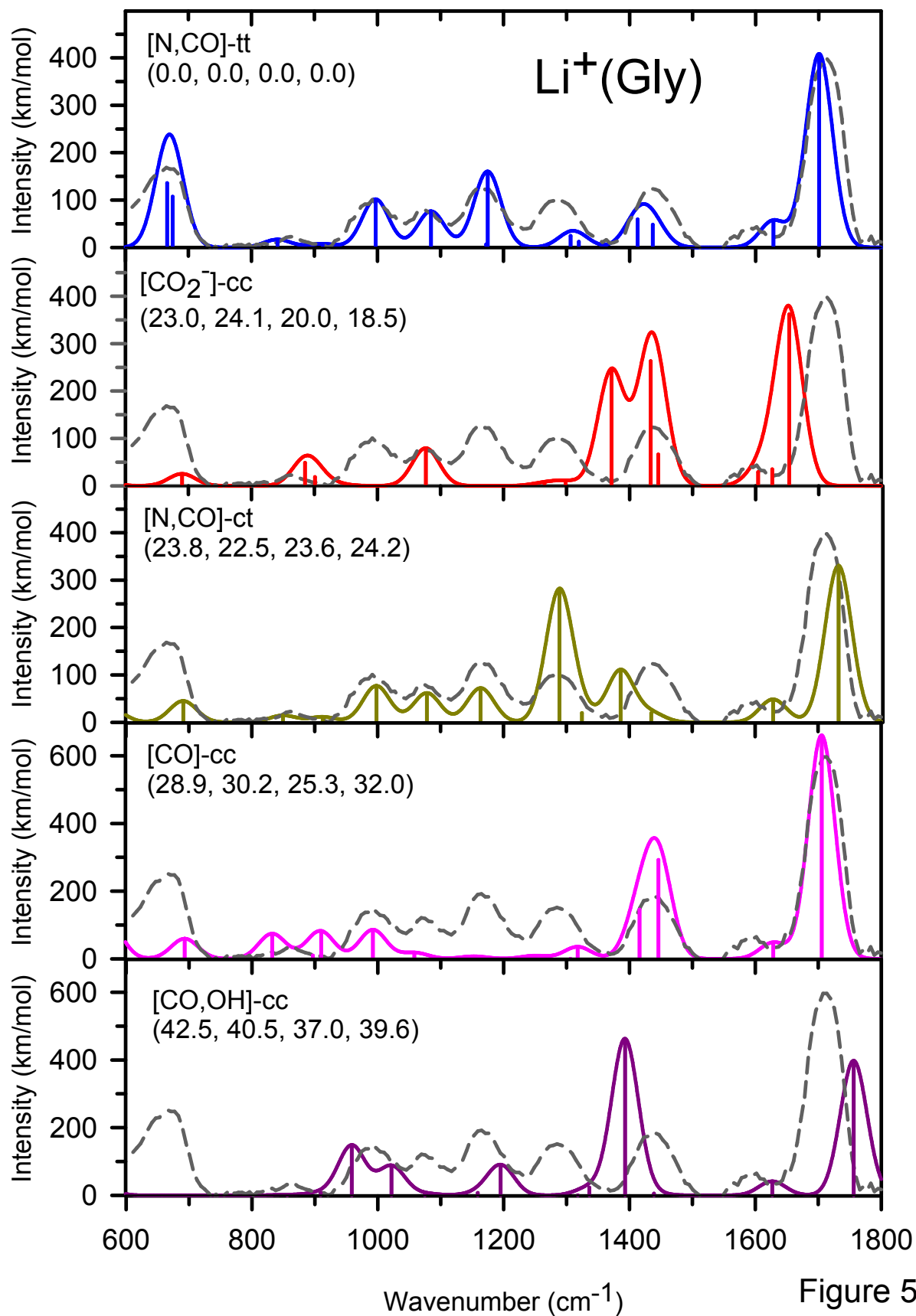


Figure 4



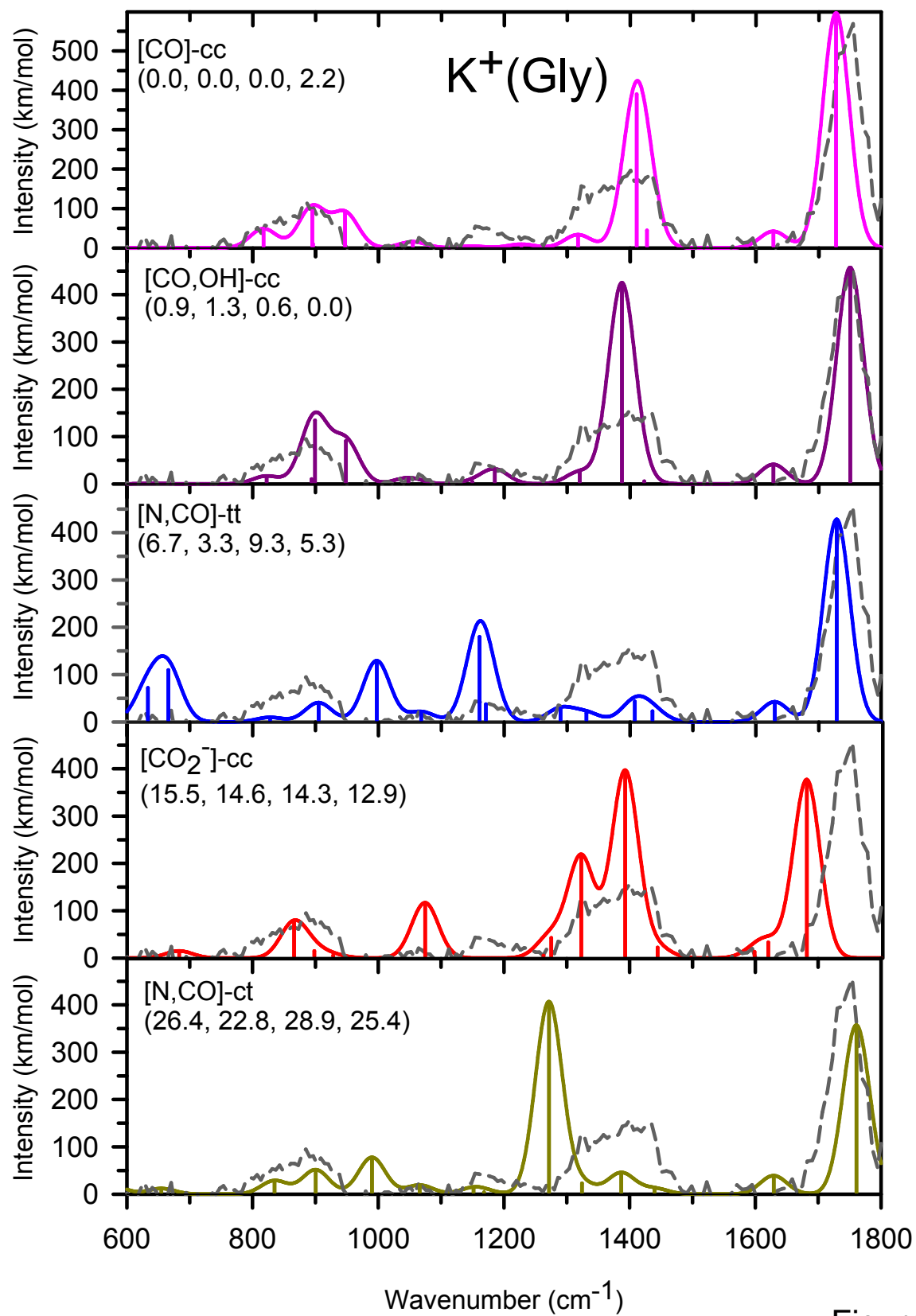


Figure 6

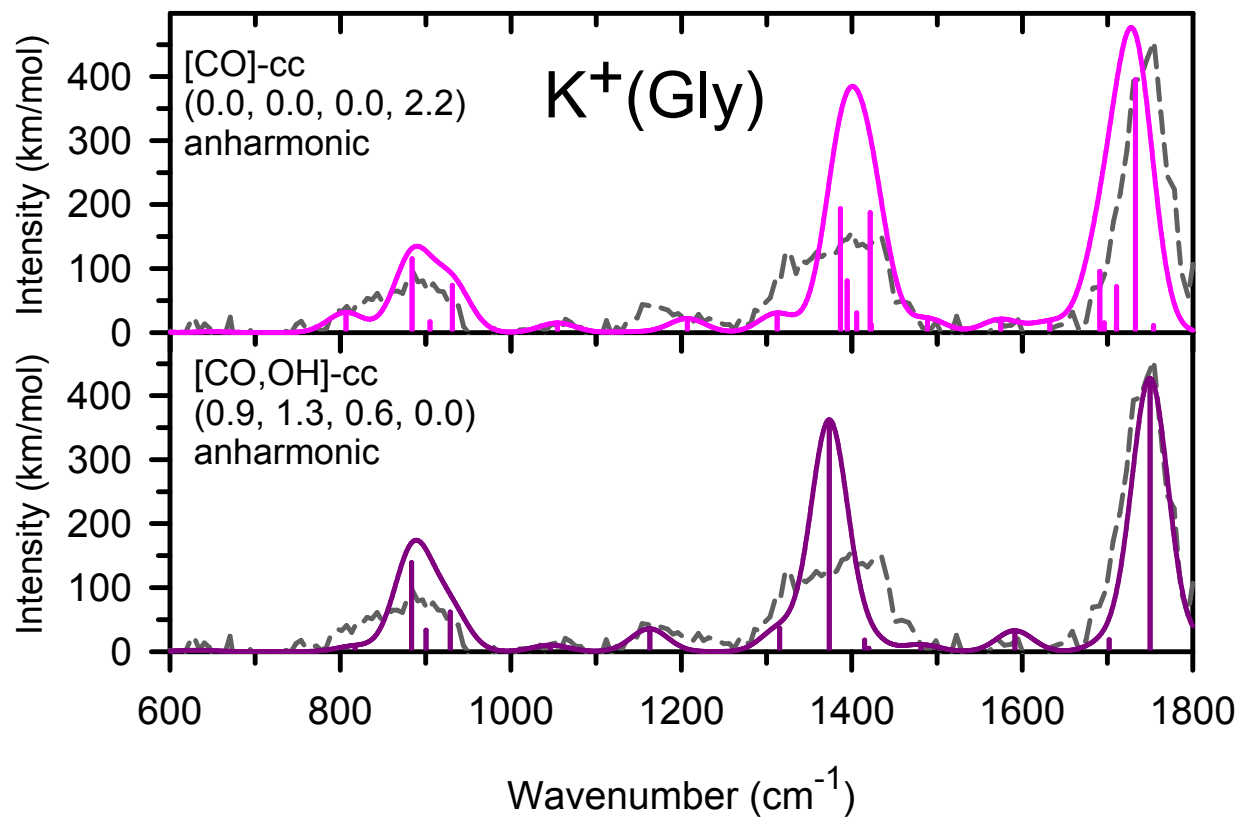


Figure 7

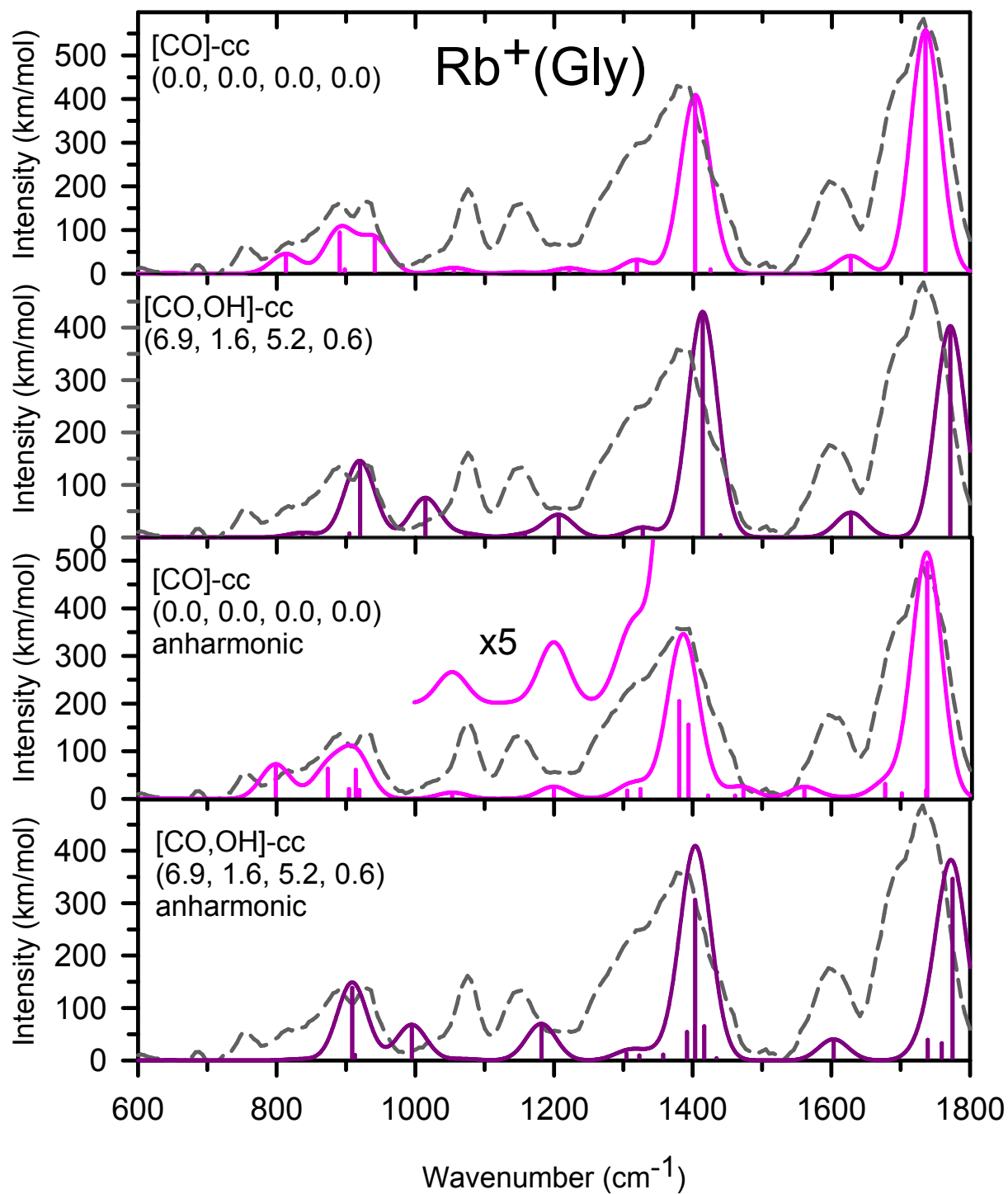


Figure 8

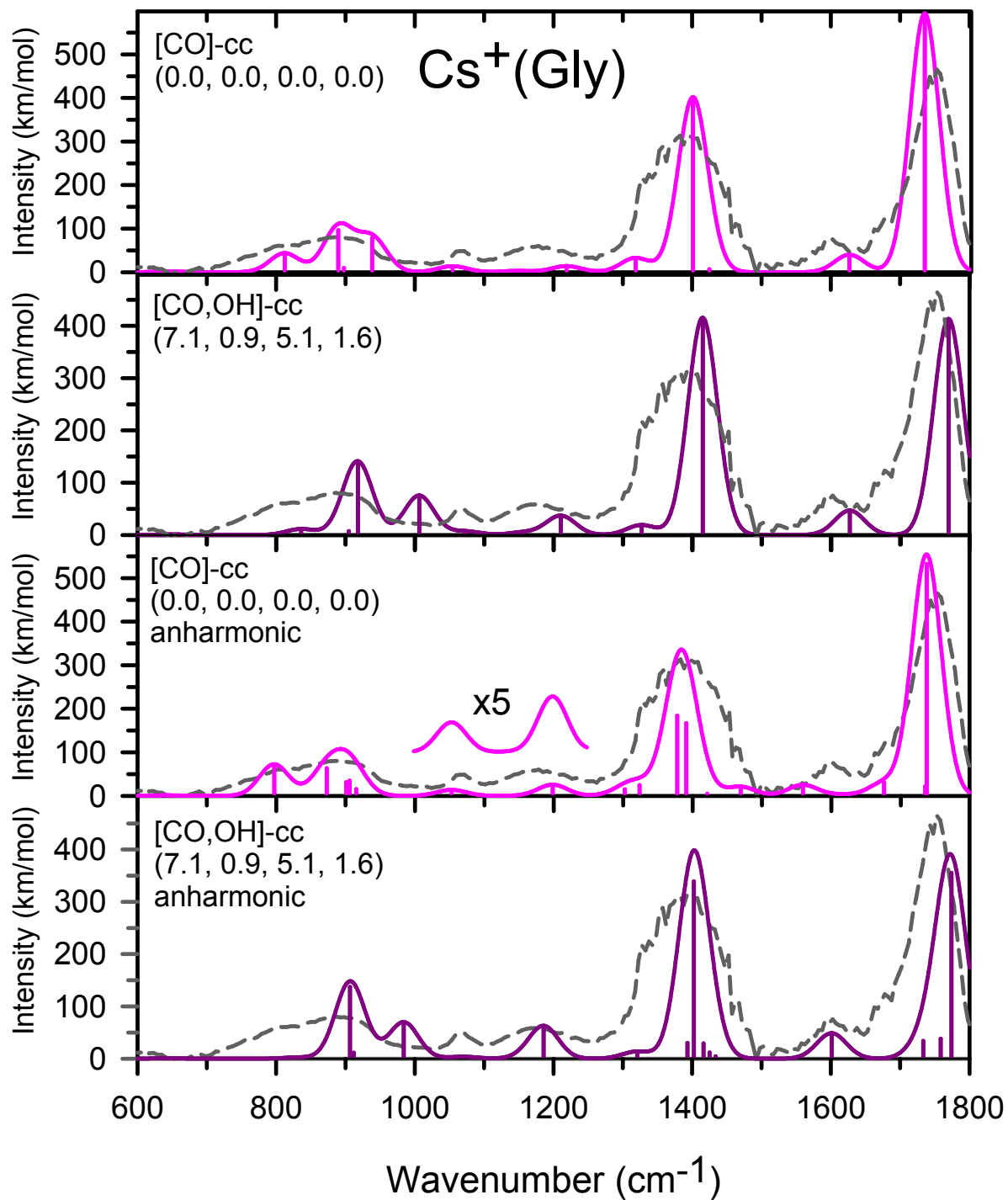
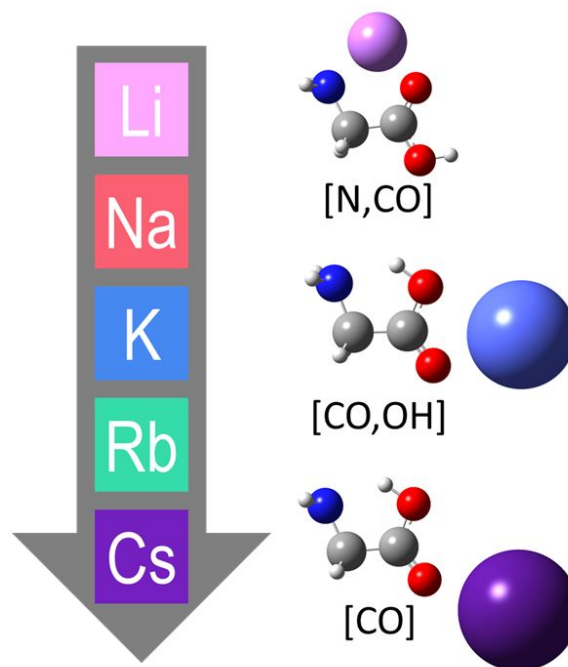
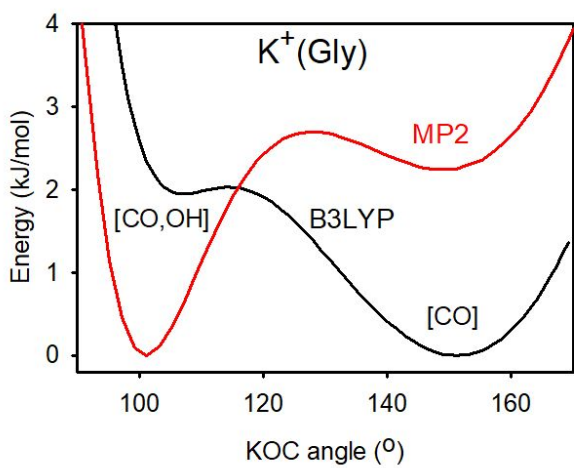


Figure 9

Table of Contents Graphic



Supporting Information for

Infrared Multiple Photon Dissociation Spectroscopy of Cationized Glycine: Effects of Alkali Metal Cation Size on Gas-Phase Conformation

P. B. Armentrout, Brandon C. Stevenson, Maryam Ghiassaei, Georgia C. Boles, Giel Berden, and Jos Oomens

Figure Captions

Figure S1: Infrared multiple photon dissociation action spectra of $M^+(\text{Gly})$ complexes where $M^+ = K^+, Rb^+, \text{ and } Cs^+$ taken on the FTICR (black trace) and QIT (red trace).

Figure S2. Relative Gibbs energies (kJ/mol) at 298 K calculated at the Level/6-311+G(2d,2p) or Level/def2TZVPP level of theory for six distinct structures of $M^+(\text{Gly})$, where $M^+ = Li^+, Na^+, K^+, Rb^+, \text{ and } Cs^+$ as a function of the alkali-metal cation relative to the energy of the most stable structure. Level includes B3LYP, B3LYP-GD3BJ, B3P86, and MP2(full).

Figure S3: Relaxed potential energy surface scans of the MOC bond angle in $M^+(\text{Gly})$ calculated at the B3LYP, B3LYP-GD3BJ, and MP2(full) levels of theory for $M = Li, Na, K$ (6-311+G(d,p) basis set) and $M = Rb, Cs$ (def2TZVP basis set). Horizontal lines indicate the relative energies including zero-point energies of the stationary states.

Figure S4: Comparison of the experimental IRMPD action spectrum for $Rb^+(\text{Gly})$ and $Cs^+(\text{Gly})$ (dashed line) with harmonic IR spectra for five structures predicted at the B3LYP/def2TZVP level except for [CO,OH]cc, which were calculated at the MP2/def2TZVP level. Relative Gibbs energies (kJ/mol) at 298 K are provided at the B3LYP, B3LYP-GD3BJ, B3P86, and MP2 levels.

Table S1: 0 K Relative Gibbs Energies (kJ/mol) of Low-Lying Conformers of M⁺(Gly) Calculated at B3LYP, B3LYP-GD3BJ, B3P86, and MP2(full) Levels of Theory^a

Structure	Li ⁺ (Gly)	Na ⁺ (Gly)	K ⁺ (Gly)	Rb ⁺ (Gly)	Cs ⁺ (Gly)
[N,CO]tt	0.0, 0.0, 0.0, 0.0	0.0, 0.0, 0.0, 0.0	3.9, 0.2, 6.4, 2.8 (1.4)	7.8, 4.1, 10.7, 6.4	11.3, 7.5, 13.4, 7.9
[CO ₂ -]cc	21.5, 0, 23.7, 18.6, 17.0	10.5, 13.5, 7.4, 7.6	12.1, 11.1, 10.9, 9.9	19.4, 18.3, 17.6, 14.5	22.0, 20.5, 19.3, 14.4
[N,CO]ct	22.3, 21.8, 22.2, 22.7	21.5, 21.2, 21.3, 21.8	23.8, 19.9, 26.4, 23.2	26.9, 23.0, 29.6, 26.5	28.9, 25.1, 31.0, 26.2
[CO]cc	29.2, 31.5, 25.6, 32.2	10.4, 13.7, 6.2, 11.8	0.0, 0.1, 0.0, 2.6 (2.1)	0.0, 0.0, 0.0, 2.1 (0.8)	0.0, 0.0, 0.0, 0.7 (0.0)
[CO,OH]cc	41.3, ^b 41.9, ^b 35.8, ^b 38.4 ^b	10.7, 13.7, 6.5, 9.1	0.6, 0.0 , 0.3, 0.0 (0.0)	4.2, ^b 0.1, ^b 2.4, ^b 0.0^b (0.0)	4.7, ^b 0.4, ^b 2.7, ^b 0.0^b (0.6)
[N,OH]tc	45.5, 43.2, 47.7, 39.1	41.3, 39.4, 42.9, 35.7	41.9, 36.0, 45.8, 35.7	45.0, 39.1, 49.1, 39.3	47.6, 41.5, 51.0, 40.8
[CO]tc	70.6, 73.5, 71.0, 75.7	49.0, 53.1, 48.5, 51.6	35.3, 36.0, 39.0, 38.8	36.7, 40.2, ^c 41.2, 40.1	33.2, 33.7, 37.3, 36.2
[CO]ct	72.5, 75.1, 72.5, 77.3	50.0, 53.7, 49.4, 52.6	37.4, 37.7, 40.9, 40.7	36.3, 36.5, 39.7, 41.2	34.8, 35.0, 38.5, 37.5
[N]tt	87.0, 86.9, 84.4, 81.8	61.5, 62.5, 60.0, 57.6	50.6, 48.0, 52.8, 47.5	49.1, 46.7, 51.7, 47.1	47.9, 45.1, 50.3, 47.0

^a B3LYP, B3LYP-GD3BJ, B3P86, and MP2 (full) (CCSD(T,full)) values calculated using the 6-311+G(2d,2p) or def2-TZVPP basis set with the structures and zero-point energies calculated at the B3LYP/6-311+G(d,p) or B3LYP/def2-TZVP level of theory. Bold indicates the ground state. ^b Collapses to [CO]cc. Values are single point calculations using MP2(full)/6-311+G(d,p) or MP2(full)/def2-TZVP structures and zero-point energies. ^c Collapses to [N,CO]tt. Value is single point calculation using B3LYP/def2-TZVP structure and zero-point energy.

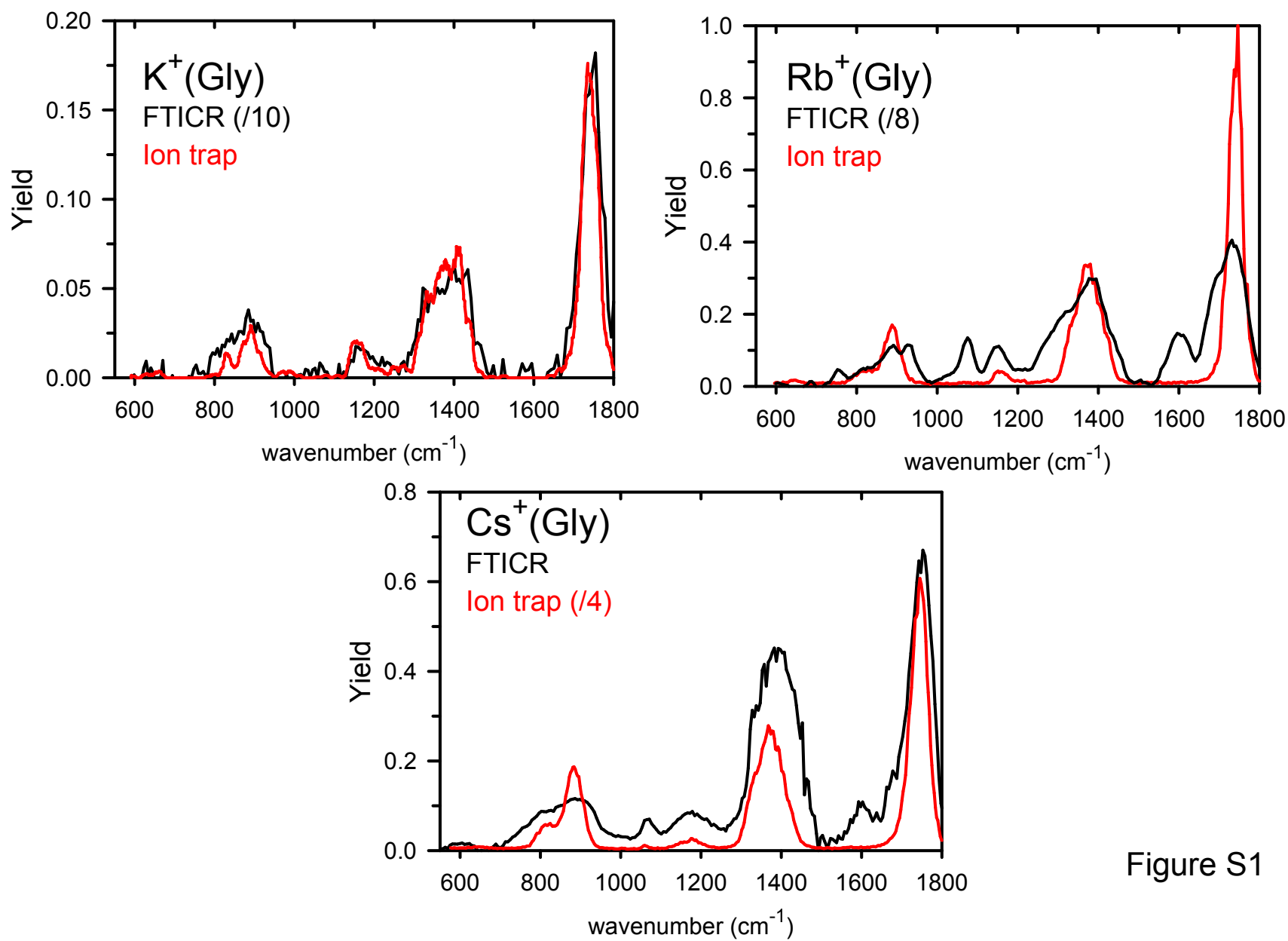


Figure S1

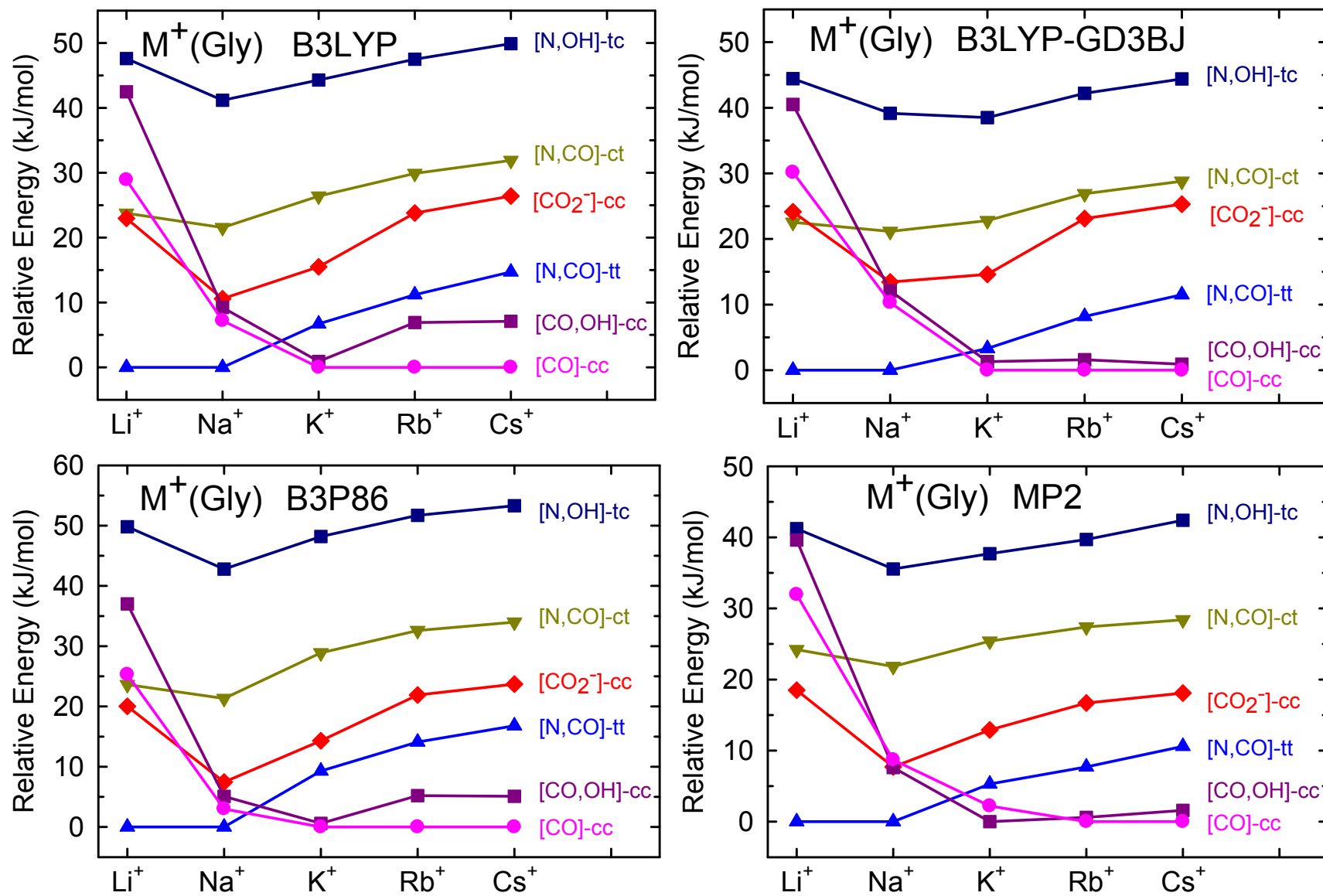


Figure S2

S5

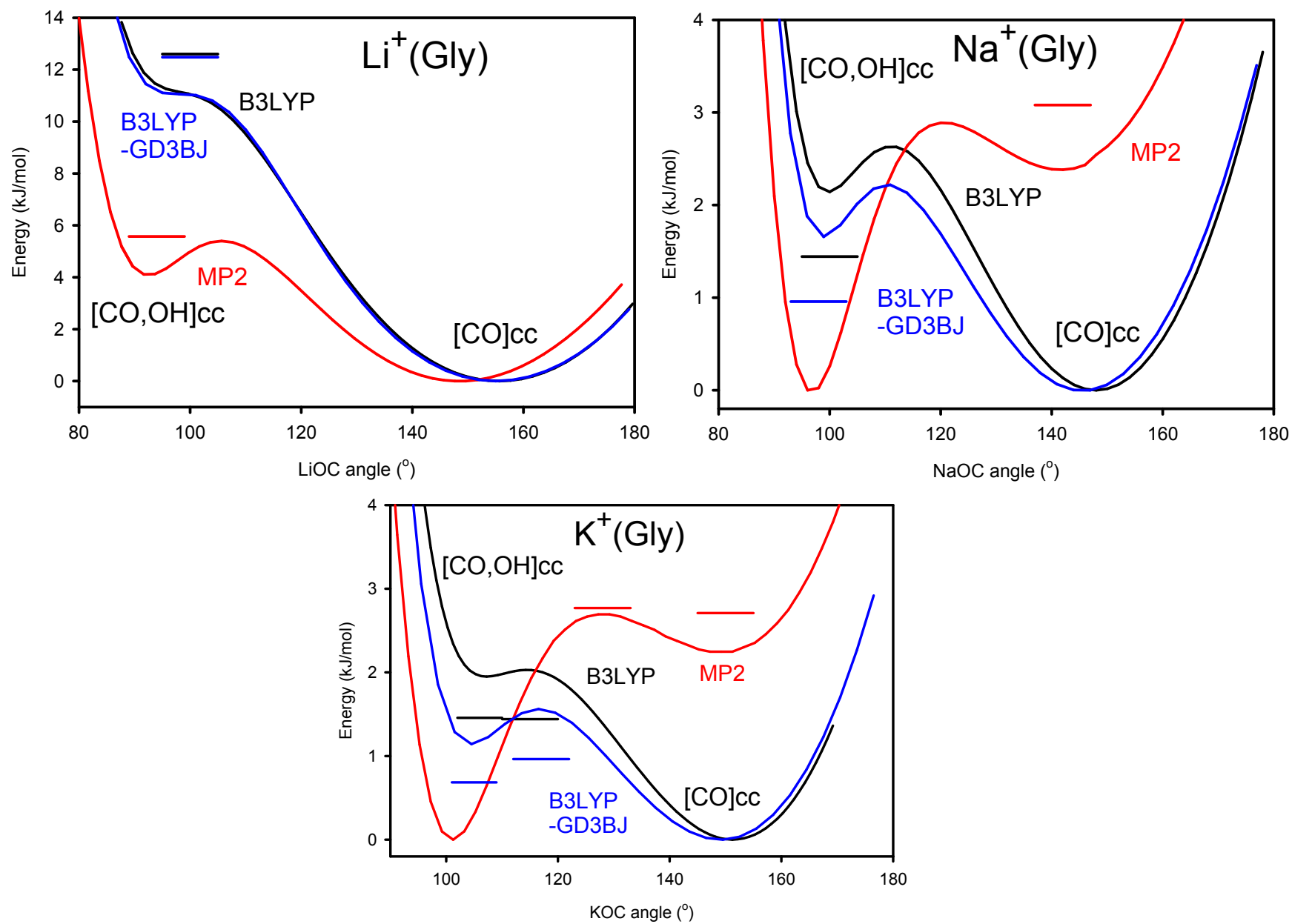


Figure S3

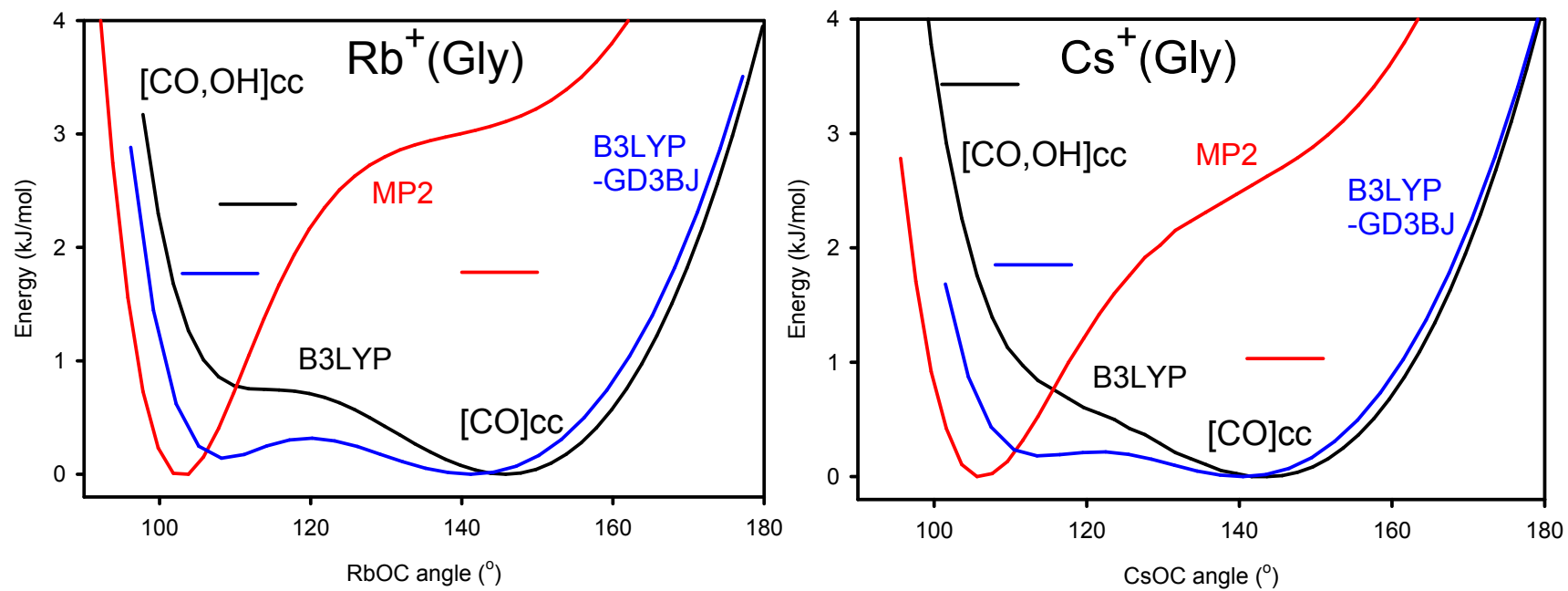


Figure S3

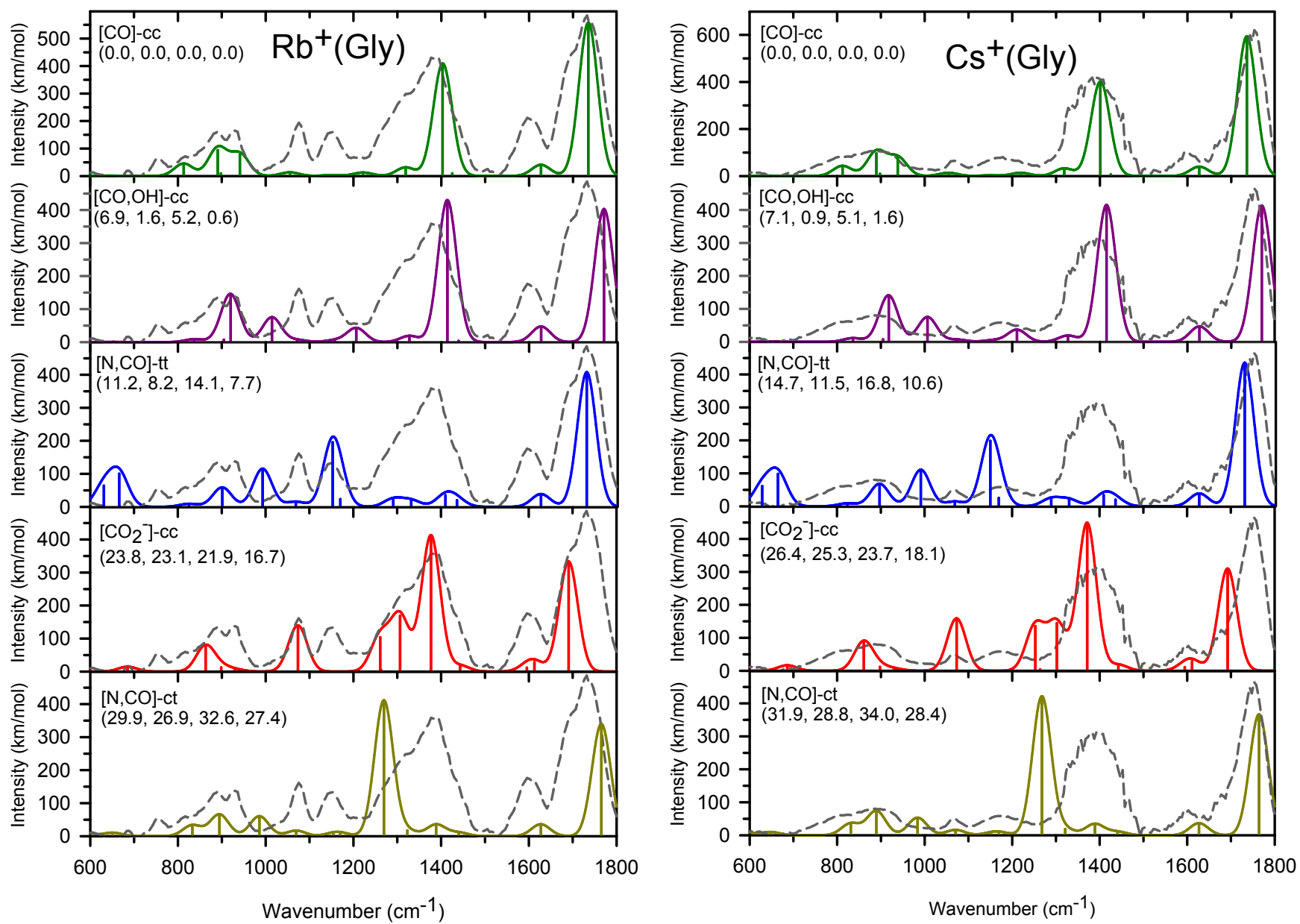


Figure S4